Quaternary Science Reviews 78 (2013) 209–224

Contents lists available at ScienceDirect

Quaternary Science Reviews

journal homepage: www.elsevier.com/locate/quascirev

Low latitude hydro-climatic changes during the Plio-Pleistocene: evidence from high resolution alkane records in the southern South China Sea

Li Li [a,*], Qianyu Li [a,b,*], Jun Tian [a], Hui Wang [a], Pinxian Wang [a]

[a] State Key Laboratory of Marine Geology, Tongji University, Shanghai 200092, China
[b] School of Earth and Environmental Sciences, University of Adelaide, SA 5005, Australia

ARTICLE INFO

Article history:
Received 23 February 2013
Received in revised form
2 August 2013
Accepted 12 August 2013
Available online 11 September 2013

Keywords:
Plio-Pleistocene
Plant *n*-alkanes
n-Alkane chain lengths
Hydro-climate

ABSTRACT

High resolution records of long chain *n*-alkane biomarkers from the southern South China Sea reveal tightly response of *n*-alkane distribution to hydro-climate changes over the past 5 Ma, with increasing longer chain *n*-C_{31} alkanes indicating a correlation with drier conditions and increasing shorter chain *n*-C_{27} alkanes with wetter conditions. The variations of the C_{31}/C_{27} ratio, or the alkane chain length index, imply humid conditions before 2.9 Ma, progressively reduced moisture since then and to bigger fluctuations between wet and dry conditions since 1.2 Ma. This long term hydro-climate trend is superimposed by glacial dry and interglacial wet patterns over the Plio-Pleistocene glacial cycles. Combined with other proxy records, our results indicate that precipitation over the tropical Asia-Pacific strengthened before the onset of the northern hemisphere glaciation and the mid-Pleistocene climate transition at about 1.2 Ma. These dramatic humidity changes over major climate transitions imply a crucial role of tropical hydrology dynamics on global climate change in the late Cenozoic.

1. Introduction

The Late Cenozoic shaped the fundamentals of today's vegetation and hydro-climate on Earth. Over the last 5 Ma, two time intervals are extremely critical (Zachos et al., 2001; Raymo et al., 2006): (1) at about 2.7 Ma, major global cooling leading to expansion of northern hemisphere glaciation, and (2) since ~0.9 Ma, intensive global ice waxing and waning in response to changes in climate from 40 ka to 100 ka cycles. Yet, how the terrestrial system responded to these climate perturbations and how hydrology and climate systems interacted during the late Cenozoic are poorly understood due to the scarcity of long term high resolution records.

Long-chain *n*-alkanes (C_{24}–C_{35}) with predominance of odd-carbon-numbered members are important lipid constituents of epicuticular waxes in land plant (Eglinton and Hamilton, 1967). Although various plants possess similar leaf lipid compositions, their typical alkyl molecular distributions are often different. As summarized in Table 1, many studies have revealed the alkane chain length variation as a function of plant types, temperature, and humidity, in addition to latitude. Grassland plant waxes contain more *n*-C_{31} alkanes, while leaf lipids from forest trees and shrubs have more *n*-C_{27} and/or *n*-C_{29} alkanes (Cranwell, 1973; Cranwell et al., 1987; Meyers and Ishiwatari, 1993; Zech et al., 2009). Differences in long-chain *n*-alkanes distribution can even distinguish species within a genus (Medina et al., 2006; Rommerskirchen et al., 2006b). Generally, warm or tropical regions favor the synthesization of longer-chain compounds, while more shorter-chain compounds are frequently produced in cooler or temperate regions (Gagosian and Peltzer, 1986; Poynter et al., 1989; Kawamura et al., 2003; Bendle et al., 2007). This has been supported by observations that a positive relationship exists between chain alkane variability and ambient temperature, with longer chain alkane synthesized often during summer, because the increasing boiling point of the high molecular weight alkanes will protect the plants standing against the external high temperature (Kawamura et al., 2003; Bendle et al., 2007; Cui et al., 2008). However, increases of longer chain length compounds in relative higher latitudes in western Africa and South America (Rommerskirchen et al., 2003, 2006a,b; Schefuß et al., 2003; Horikawa et al., 2010; Vogts et al., 2012) may cast doubts on a wider application of this latitudinal correlation with alkane chain length variability found mainly in the western Pacific (Kawamura et al., 2003; Sachse et al., 2006; Bendle

* Corresponding authors. State Key Laboratory of Marine Geology, Tongji University, Shanghai 200092, China.
E-mail addresses: lilitju@tongji.edu.cn (L. Li), qli01@tongji.edu.cn (Q. Li).

0277-3791/$ – see front matter © 2013 Elsevier Ltd. All rights reserved.
http://dx.doi.org/10.1016/j.quascirev.2013.08.007

Table 1
A synthesis of alkane chain length distribution ($>C_{23}$) as revealed in various studies.

Area	Location	Materials or periods	Index	Distributional features of longer chain length alkyl lipids		References
Eastern Mediterranean (Cretan Sea)	25°06′E Transect, 35°23′ −40′N, 25°20′E Transect, 35°23′ −40′N	Surface sediments	C_{29}/C_{31}	Spatial	Off shore areas	Gogou et al., 2000
Northern Atlantic (Island of Bermuda)	32°20′N, 64°45′W (Nov., 1995–Aug., 1998)	Aerosols	C_{29}/C_{31}	Seasonal	Source difference and aridity	Conte and Weber, 2002
Western North Pacific	27°4′N, 142°13′E	Aerosols	$ACL_{C_{27}-C_{35}}$	Seasonal	Later summer → Temperature	Kawamura et al., 2003
Western Pacific	6°S, 27°N, 43°N	Plant	$ACL_{C_{27}-C_{33}}$	Latitudinal	Relative lower latitude → Higher temperature	Kawamura et al., 2003
Southeastern Atlantic Continental Margin	30°S–4°S	Surface sediments	$ACL_{C_{27}-C_{33}}$; $C_{31}/(C_{29}+C_{31})$	Latitudinal	Relative higher latitude → Aridity, seasonality	Rommerskirchen et al., 2003
West Africa Coast	10°S–30°N	Dusts	$C_{31}/(C_{29}+C_{31})$	Latitudinal	Relative higher latitude → Aridity, not temperature or vegetation	Schefuß et al., 2003
The Pyrenees	0°45′E Transect, 42°N–43°N, Elevation: 1600–2300 m	Plants	Weighted average chain of odd *n*-alkane ($C_{29}-C_{35}$)	Elevational	Lowermost and uppermost elevations	Dodd and Poveda, 2003
Chinese Loess Plateau	34°–38°N, 107°–110°E	Plants	C_{31}/C_{29} C_{31}/C_{27}	Vegetational	More grass → Higher wetter conditions	Liu and Huang, 2005
Northern Europe	41°N–69°N	Plants	$ACL_{C_{25}-C_{31}}$	Latitudinal	Low latitude → Higher temperature and precipitation	Sachse et al., 2006
Southeastern Atlantic Continental Margin	4°S–30°S	Sediments	$ACL_{C_{27}-C_{33}}$	Latitudinal	Higher latitude → Aridity	Rommerskirchen et al., 2006a
Southern Africa	20°S–35°S	Plants	$ACL_{C_{27}-C_{35}}$	Vegetational	C_4 Grass → Warm and arid condition	Rommerskirchen et al., 2006b
Western Pacific and Southern Ocean	65°S–27°N	Aerosol	$ACL_{C_{25}-C_{35}}$	Latitudinal	Tropics → High temperature	Bendle et al., 2007
Northern Ecuador (The Andes)	0°35.68′N, 77°41.6′W	Soil	C_{29}/C_{31}	Vegetational	Tropical alpine grassland	Jansen et al., 2008
South China	30°26.74′N, 110°25.17′E	Plants	$ACL_{C_{23}-C_{37}}$	Seasonal	Summer → Higher temperature	Cui et al., 2008
Eastern Tropical Pacific	95°W Transect, 10°N–10°S	Surface sediments	$C_{31}/(C_{29}+C_{31})$ $ACL_{C_{27}-C_{33}}$	Latitudinal	Relative high latitude → Hot and dry environment	Horikawa et al., 2010
China	22°N–39°N	Plants	$ACL_{C_{25}-C_{33}}$	Vegetational and Latitudinal	Grasses > Trees Lower latitude → Higher temperature	Duan and He, 2011
Eastern China	18°N–50°N	Surface soils	C_{27}/C_{31}; $ACL_{C_{25}-C_{33}}$	Latitudinal	Higher latitude and aridity	Rao et al., 2011
Southwest Africa Margin	28°S–1°N	Surface sediments	$ACL_{C_{25}-C_{35}}$	Latitudinal and humid	Higher latitude → Aridity	Vogts et al., 2012
Central China (Erxianyan Peatland)	29°43.54′N, 108°48.18′E	*Sphagnum* plants and peatland	$ACL_{C_{21}-C_{33}}$	Hydrological gradient	Aridity	Huang et al., 2012
Lake Baikal (Core 323-PC1)	55°32.08′N, 109° 31.28′E	0–20 ka	C_{27}/C_{31}	Glacial → Herbaceous		Brincat et al., 2000
Central Europe (Lake Steisslingen)	47°47′N, 8°55′E	10 ka–16 ka	$C_{31}/(C_{27}+C_{29}+C_{31})$	Cold periods		Schwark et al., 2002
South China (Two Profiles In Vermicular Red Earth)	29°9.83′N, 114°41.88′E; 29°9.8′N, 114°42.22′E	0–800 ka	C_{27}/C_{31}	Cold and dry periods		Xie et al., 2003
South China Sea (17962)	7°11′N, 112°5′E	0–30 ka	C_{27}/C_{31}; C_{27}/C_{31}	Glacial → Aridity		Hu et al., 2003
Central Italy, Lake Albano (Core PALB94-3A)		0–12 ka	$(C_{27}+C_{29})/\sum(C_{23}-C_{33\text{-odd c}})$	Early Holocene → Warm and wet		Hanisch et al., 2003
Tasman Sea (Fr94-Gc3)	44°15′S, 149°59′E	0–470 ka	$ACL_{C_{25}-C_{31}}$	Glacials → Aridity		Calvo et al., 2004
South China (Dingnan peat)	24°15′N, 115°2′E	0–18 ka	$ACL_{C_{27}-C_{33}}$	Wet and warm periods		Zhou et al., 2005
Chinese Loess Plateau (Xifeng)	35°46′N, 107°41′E	0–130 ka	C_{31}/C_{29} C_{31}/C_{27}	Interglacials → Grassland increasing → Warm and wet climate		Liu and Huang, 2005
Chinese Loess Plateau (Xunyi and Luochuan)	Xunyi (35°20′N, 106°18′E); Luochuan (35°45′N, 109°24′E)	0–170 ka	$C_{31}/(C_{29}+C_{31})$	Warm interglacials → Higher precipitation and temperature		Zhang et al., 2006
North Pacific	49°44.70′N, 168°18.93′E	0–350 ka	$ACL_{C_{27}-C_{31}}$	Beginning of the interglacial → Aridity		Ratnayake et al., 2006
Southeastern Atlantic Continental Margin	4°S–30°S	0–135 ka	$ACL_{C_{27}-C_{33}}$	Glacials → Aridity		Rommerskirchen et al., 2006a
Equatorial East Africa (Mt. Kilimanjaro)	~3°S, 37°E	0.8–18.8 ka	C_{31}/C_{27}	Cold and dry climate		Zech, 2006
Western China (Zoigê-Hongyuan peat)	32°48′N, 102°32′E	0–11.4 ka	$(C_{27}+C_{29}+C_{31})/\Sigma C_{23-31\text{-odd}}$	Cold and dry events		Zheng et al., 2007
South American (Arg. D4)	27°23.58′S, 55°31.87′W	0–~50 ka	C_{31}/C_{27}	Grassland and dry climate		Zech et al., 2009
Southeast Africa (Lake Malawi, M98-1P)	10°15.99′S, 34°19.19′E	0–23 ka	$ACL_{C_{23}-C_{33}}$	Holocene → Higher temperature		Castañeda et al., 2009
South China (Dingnan)	24°45′N, 115°02′E	0–16 ka	$C_{31}/(C_{27}+C_{29}+C_{31})$	Cool and dry periods		Zheng et al., 2009
Eastern Tropical Pacific (HY04)	4°1.66′N, 95°3.45′W	0–740 ka	$C_{31}/(C_{29}+C_{31})$	Glacials → Aridity		Horikawa et al., 2010

Northeast China (Hani Peat Bog)	42°13′N, 126°31′E	0–16 ka	C_{27}/C_{31}; C_{29}/C_{31}; C_{33}/C_{31}; $ACL_{C_{27}-C_{31}}$	Early Holocene → Humidity	Yamamoto et al., 2010
Southern Africa (Spitzkoppe Midden, SP)	21°49′S, 15°11′E	0–12 ka	$C_{31}/(C_{29}+C_{31})$	Early Holocene → Humidity	Carr et al., 2010
Central America (Costa Rica, Lm1)	9°29.67′N, 83°29.23′W	0–13 ka	$ACL_{C_{21}-C_{33}}$	Holocene → Aridity	Lane et al., 2011
South China Sea (MD97-2146)	20°7.08′N, 117°23.02′E	0–30 ka	$ACL_{C_{25}-C_{33}}$	Glacials → Aridity	Shintani et al., 2011
Tibetan Plateau (Linxia Basin)	102°30–104° E, 35°10–35°51′N	4.3–23 Ma	C_{27}/C_{31}; C_{17-21}/C_{27-31}	Arid-cold conditions	Wang et al., 2012
South China Sea (MD05-2904)	20°8.07′N, 117°21.61′E	0–30 ka	$ACL_{C_{25}-C_{33}}$, C_{31}/C_{27}	Glacials → Aridity	Zhou et al., 2012

et al., 2007). Apart from temperature, moisture is also a crucial factor on the biosynthesis of leaf lipids, as longer chain length alkanes are synthesized to prevent water loss at arid conditions (Dodd and Afzal-Rafii, 2000). Studies on the hydrogen isotope of leaf wax lipids also corroborate that longer alkane chain compounds provide a better protection from evaporative water loss (Liu and Huang, 2005; Sachse et al., 2006). A close examination of the data from the above three regions with contradicted latitudinal distribution of alkane chain lengths indeed reveals a strong association of increasing alkane chain length with arid continental environments regardless of their location from the equator, and the high value of alkane chain length from the western Pacific appears not only associate with high temperature but also with the arid region in Australia. Analyses of surface soils from East China also show that increases in the longer chain alkanes are always correlated with low precipitation (Rao et al., 2011). Clearly, regional hydro-climatic factors exert a more important role in delineating the alkane chain length distribution in plants.

Meanwhile, featuring chemical inertness and resistance to biodegradation, these alkanes are common components in eolian dusts, lacustrine and marine sediments and are excellent biomarker compounds to be used for tracking continental vegetation changes in response to climate change (Eglinton and Eglinton, 2008), as revealed by many recent studies (Table 1). For example, the glacial enrichment of longer chain alkanes in the vermicular red earth in South China (Xie et al., 2003) and in marine sediments from the Tasman Sea (Calvo et al., 2004) and from the eastern equatorial Pacific (Horikawa et al., 2010) together imply a controlling role of dry climate rather than cold temperature during glacial periods on regional alkane chain length distribution. However, the late Quaternary vegetation history in southeast Africa illustrated a positive correlation between temperature and chain length change, with increases in longer chain length corresponding to higher temperature (Castañeda et al., 2009). Similar phenomena have also been observed in Chinese Loess Plateau and northeast China peat records (Liu and Huang, 2005; Zhang et al., 2006; Yamamoto et al., 2010). These works demonstrate the ability of plants to alter the chain length in their leaf waxes to minimize evaporation of water vapor from their leaves, when temperature is high and/or moisture reduces (Yamamoto et al., 2010). Therefore, the distribution of higher plants leaf wax can provide useful information relating to climate change, especially the temperature and hydrological changes on land (Calvo et al., 2004; Hughen et al., 2004; Bendle et al., 2007; Horikawa et al., 2010; Yamamoto et al., 2010).

The modern southern South China Sea is a semi-enclosed basin bordered by the Indochina peninsula, Malaysia, Sumatra and Borneo (Fig. 1B). Studies have shown that the terrestrial contribution to South China Sea deposits was mainly from riverine input, much less so from eolian supply (Wang, 1999). Presently, the Mekong River and rivers in the Malay Archipelago are the main source of terrigenous sediments in the southern South China Sea. During glacials at ~−120 m low sea level, however, large drainage systems developed on the exposed Sunda Shelf, especially the Paleo-Sunda River or Molengraaff River, may have acted as the extra important sediment source (Wehausen et al., 2003; Sendjaja and Kimura, 2010; Wan et al., 2006, 2010). Located within the influence of Western Pacific Warm Pool, this area is characterized by a non-seasonal climate with the average annual temperature of about 25–30 °C, annual precipitation higher than 2000 mm and the tropical rainforest as the dominant vegetation type (Heaney, 1991; Sun et al., 2000). However, whether the southern South China Sea during glacials was drier or not is still a subject of debate (Wang et al., 2009 and references therein). No arid climate had occurred in Sunda Land during the Last Glacial Maximum according to the steady carbon isotope of the leaf waxes (Hu et al., 2003). On the contrary,

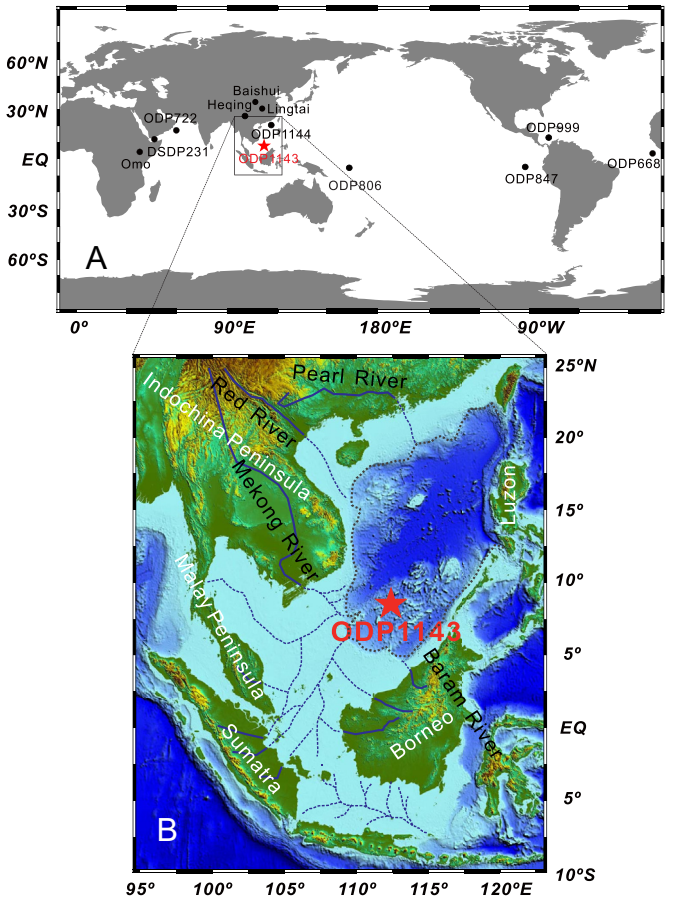

Fig. 1. (A) Schematic map showing the locations of ODP Site 1143 and other sites mentioned in the text. (B) The imbedded South China Sea map denoted the glacial shoreline (dashed gray line) and the glacial drainage systems on the exposed Sunda shelf (blue dashed line) during in the Last Glacial Maximum. (For interpretation of the references to color in this figure legend, the reader is referred to the web version of this article.)

climate modeling based on relative cooler mean temperatures and reduced evaporation, together with the imaged "savanna corridor" in the central Sunda Land marked by large scale savanna growth due to reduced rainfall and increased seasonality, during the Last Glacial period by multi-proxies data (Heaney, 1991; Gasse, 2000; De Deckker et al., 2002; Bird et al., 2005) suggest increased aridity globally during glacial periods, including the Warm Pool region. Thus, new arrays of evidences from long sediment records are needed to depict hydro-climate conditions in the southern Asia over late Cenozoic glacial cycles. As long-chain *n*-alkanes from deep sea sediment cores are likely to reveal changes in terrigenous material flux by rivers under the influence of climate, sea level and precipitation, we investigate in this study *n*-alkane variability in a sediment core recovered from the southern South China Sea, and discuss the implications of temporal variations in terrigenous higher plants alkane flux over the last 5 Ma in the region.

2. Materials and methods

Ocean Drilling Program (ODP) Site 1143 (9°21.72′N, 113°17.11′E; water depth 2772 m) lies in the southern part of the South China Sea (Fig. 1; Wang et al., 2000). A total of 1600 samples were taken at 10 cm intervals for analyses of terrestrial alkanes. The average temporal resolution by samples is ~3 ka based on the orbitally tuned foraminifer $\delta^{18}O$ age model (Tian et al., 2002).

Methods for lipid analysis were described in details elsewhere (Li et al., 2011). Briefly, about 5 g freeze-dried samples were extracted ultrasonically four times by dichloromethane/methanol (3:1, V/V), after adding an internal standard (*n*-$C_{24}D_{50}$ alkane). After saponification, neutral components were recovered and then separated into nonpolar and polar fraction by silica gel column. The nonpolar fraction (alkanes) was measured by gas chromatography (GC, Trace GC 2000, Finnigan, Thermo Electron) equipped with HP-1 capillary column (50 m × 0.32 mm × 0.17 μm, J&W) and flame ionization detector. Both the injector and detector were set at 300 °C. Helium was used as the carrier gas with a flow rate of 1.2 ml/min by splitless injecting. The oven was kept initially at 80 °C for 1 min, then was programmed to 200 °C at 25 °C/min, followed by 4 °C/min to 250 °C, then 1.8 °C/min to 300 °C (maintained for 8 min), 5 °C/min to 310 °C (maintained for 5 min). Some of the samples were performed on gas chromatography–mass spectrograph (GC–MS) to confirm no co-eluting existence. The temperature program used is the same as aforementioned. All the analyses and measurements were undertaken in the State Key Laboratory of Marine Geology at Tongji University, China.

3. Results

3.1. Distribution of plant-wax in ODP Site 1143 sediments

The total alkane abundances (Σalkanes) for high molecular weigh *n*-alkanes in the range of C_{24}–C_{35} varied from 69 to 833 ng/g (Fig. 2), forming a down-core trend shared also by some distinctive long-chain *n*-alkanes including *n*-C_{27} and *n*-C_{31}. In general, the profile of Σalkanes shows two distinct intervals: (a) lower values with smaller fluctuations before 0.8 Ma, ranging between 69 ng/g and 533 ng/g, or 221 ng/g on average, and (b) increasing values with large fluctuations after 0.8 Ma, oscillating from 84 ng/g to 833 ng/g, or 381 ng/g on average. Glacial–interglacial fluctuations, especially during the late Quaternary (especially after 0.5 Ma) are characterized by higher Σalkanes values in glacials and lower values in interglacials (Figs. 2 and 3). During glacials, the Σalkanes varied mainly between 400 and 800 ng/g, averaged ~500 ng/g, with high values of >750 ng/g alkanes at MIS 6, 12, and 18 (Fig. 3). During interglacials, the Σalkanes are generally lower than 350 ng/g, averaged 250 ng/g. For the early Quaternary, the glacial enrichment–interglacial deficiency features of alkanes can still be found, but exhibit much depressed fluctuations in the Σalkanes with only ~120 ng/g for most glacial–interglacial transitions, or lower than half of the values in the late Quaternary (300 ng/g). This was mainly caused by the lower Σalkanes, 220–300 ng/g, during most glacials before 1.2 Ma compared to the relative stable Σalkanes values at interglacials throughout the studied interval. As discussed below, these alkane changes correspond to the major hydro-climate stages and topographical changes in the region. To address the dilution problems, the calculated mass accumulation rate of alkanes revealed a generally parallel pattern with the content of the Σalkanes (Fig. A1), which can be used to represent the terrestrial supply over times.

3.2. Alkane index variations

Various parameters have been proposed to evaluate the alkane distribution, including carbon preference index (CPI), average carbon chain lengths (ACL) and various simplified molecular ratio (i.e. C_{31}/C_{27}; $C_{31}/(C_{27}+C_{31})$, as listed in Table 1). CPI, a mathematical expression of the odd over even predominance among high molecular weight members, potentially indicates the *n*-alkane source (Bray and Evans, 1961). An odd-numbered carbon predominance between C_{24} and C_{34}, with CPI values >1.0, is found throughout the

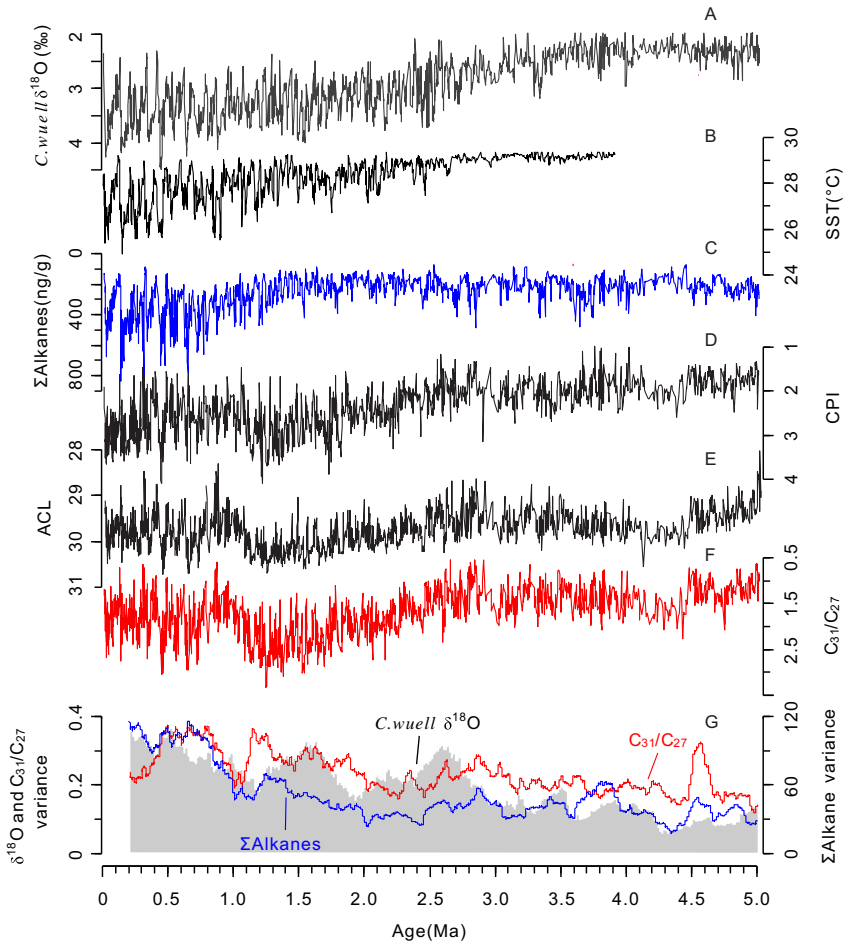

Fig. 2. Paleoclimate proxy records over the last 5 Ma at ODP Site 1143, southern South China Sea. (A) Benthic foraminifer *Cibicidoides wuellerstorfi* $\delta^{18}O$ (Tian et al., 2002), (B) Alkenone based sea surface temperature (SST) (Li et al., 2011), (C) Total alkanes of *n*-C_{24} to *n*-C_{35} (Σalkanes), (D) Carbon preference index (CPI); (E) Average carbon chain lengths (ACL); (F) Ratio of *n*-C_{31} and *n*-C_{27} alkanes (C_{31}/C_{27}), (G) 200-ka moving windows of the benthic $\delta^{18}O$ (gray shadow, left coordinate), Σalkanes (blue, right coordinate) and C_{31}/C_{27} (red, left coordinate). (For interpretation of the references to color in this figure legend, the reader is referred to the web version of this article.)

down core samples analyzed, indicating a dominant contribution from vascular plants especially during the late Quaternary.

$$\mathrm{CPI} = \left[\sum C_{25-33(\mathrm{odd})} / \sum C_{24-32(\mathrm{even})} + \sum C_{25-33(\mathrm{odd})} / \sum C_{26-34(\mathrm{even})}\right] / 2$$

Average chain length (ACL) refers to the average number of carbon atoms per molecule based on the abundance of the odd-carbon-numbered higher plant *n*-alkanes (Poynter and Eglinton, 1990), which provides an insight into alkane distribution variability. For the late Quaternary (particularly after 0.5 Ma) sediments at ODP Site 1143, the CPI and ACL of *n*-alkanes (C_{24}–C_{35}) vary at 2–4 and 28–30, respectively, consistent with previous investigations in this area (Hu et al., 2003; Pelejero, 2003).

$$\mathrm{ACL} = (C_{25} \times 25 + C_{27} \times 27 + C_{29} \times 29 + C_{31} \times 31 + C_{33} \times 33)/(C_{25} + C_{27} + C_{29} + C_{31} + C_{33})$$

Besides the ACL, various parameters have been used to evaluate the variability of alkane chain length, i.e. C_{31}/C_{27}; C_{29}/C_{31}; $C_{31}/(C_{27} + C_{31})$; $C_{31}/(C_{29} + C_{31})$; $C_{31}/(C_{27} + C_{29} + C_{31})$; $(C_{27} + C_{29})/\Sigma C_{27-33}$ (Table 1). Generally, *n*-C_{27} and *n*-C_{31} alkanes are abundant in the land plant wax, with the former dominating in trees and shrubs and the latter in herbaceous plants (Cranwell, 1973; Meyers and Ishiwatari, 1993), although this relationship is being questioned (Rao et al., 2011). These two *n*-alkanes account for 20%–30% of the total high molecular weight alkane in the present sediment archive. The discrepancy in degradation and diagenesis on individual alkanes (*n*-C_{27}, or *n*-C_{31} alkane) can be excluded because their close carbon members are present. The *n*-C_{27} and *n*-C_{31} alkanes as well as their ratios provide simple proxies for the complex alkane chain length system in plants, and therefore have been popularly used in recent paleoclimate studies (Table 1 and references therein). Because the down core patterns of ACL and C_{31}/C_{27} are similar (Fig. 2E and F), the relatively simple style of C_{31}/C_{27} is chosen to represent the alkane length index in the following discussion. We also limit our discussion to higher molecular weigh *n*-alkanes (>C_{24}) and their chain length variability which are regarded as continental plants source.

As shown in Fig. 2, the C_{31}/C_{27} ratio fluctuates between 0.5 and 3 with three stages of major changes: (a) 5–2.9 Ma with smaller fluctuations between 0.5 and 2, (b) 2.9–1.2 Ma with gradual increases from 0.5 to 3.3, and (c) after 1.2 Ma with large fluctuations between 0.6 and 3. Superimposed on these major stages are smaller-scale fluctuations with relative low and high ratio values in responding to interglacial and glacial cycles, respectively, although exceptions exist. During late Quaternary glacials, C_{31}/C_{27} ratio is 2.2 on average, reaching 3 at MIS 12, 16 and 18, while during interglacials it fluctuates mainly between 1 and 1.5. Before 1 Ma,

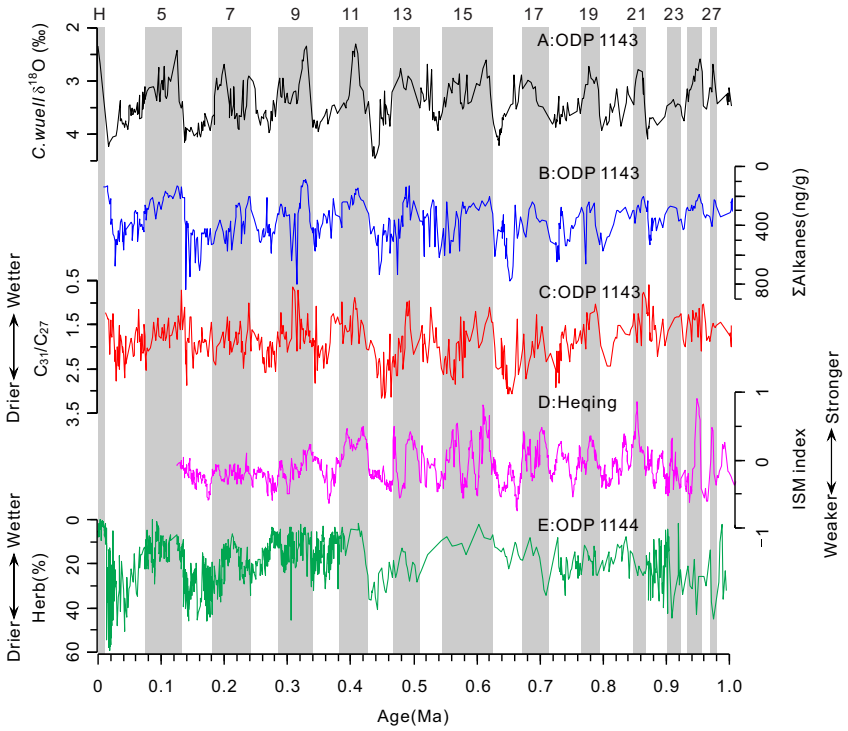

Fig. 3. Paleoclimate records for the last 1 Ma. (A) Benthic foraminifer *Cibicidoides wuellerstorfi* $\delta^{18}O$, (B) Σalkanes and (C) Ratio of C_{31}/C_{27} at ODP Site 1143, (D) Integrated Indian Summer Monsoon index (ISM) from the Heqing Basin (An et al., 2011), (E) Herb pollen percentage at ODP Site 1144 (Sun et al., 2003). Gray bars denote low C_{31}/C_{27} values corresponding to warm interglacials on odd marine isotope stages (MIS).

glacial–interglacial difference of C_{31}/C_{27} is overall stable at 1.2, although it increased from 0.55 to 2 in warm periods and from 1.74 to 3.3 in cool periods during the late Pliocene-middle Pleistocene.

4. Discussions

4.1. Source of the settled n-alkanes in the southern South China Sea and their influence on alkane index

The *n*-alkanes extracted from all down core samples show uniform distribution with homologous series of C_{24}–C_{35} alkanes, consistent with alkane composition records from continental aerosols of China and in sediments from other localities of the South China Sea (Simoneit et al., 1991; Hu et al., 2003; Pelejero, 2003; He et al., 2008; Shintani et al., 2011; Zhou et al., 2012). The most distinguishing feature is the odd to even carbon number preference. CPI is frequently used as an indication of *n*-alkane source, influenced by the type of organic matter and maturity (Bray and Evans, 1961). Generally, high CPI values represent an odd carbon number preference over even numbers, with CPI of 5–10 or more indicating from higher land plant, while CPI close to 1.0 may imply a petroleum input, a thermal alteration and/or a marine source (Mazurek et al., 1989; Hedges and Prahl, 1993; Jeng, 2006; Diefendorf et al., 2011). The present results of higher molecular weight *n*-alkanes with odd carbon predominance, especially in the late Quaternary, implied dominating terrestrial plants origins. Although recent studies had shown an insect-derived alkanes shared the same features as in epicuticular waxes of land plants, the biomass of alkanes source made by insect is lower by several orders than land vascular plants and may constitute only a minimal component to soil and deep sea settling particles (Chikaraishi et al., 2012).

Generally, the terrigenous sediment deposited in the South China Sea is transported mainly by rivers (Wang and Li, 2009). As for the ODP Site 1143, it has a similar distance with the Mekong River in the Indochina peninsula and the Baram River in Borneo. But the runoff and suspended sediment discharge from the Mekong River are 5.9 m/yr and 160.0 Mt/yr, which are considerably higher than from the Baram River with only 2.5 m/yr and 12 Mt/yr, respectively (Milliman and Meade, 1983; Hiscott, 2001; Wang and Li, 2009). Meanwhile, the NE–SW extending Borneo Trough, or Nansha Trough, may receive most of the terrigenous sediments from northern Borneo, leaving only a small portion transported continuously to the deep sea (Hiscott, 2001). Geochemical evidence, i.e., TiO_2/Al_2O_3 (Wehausen et al., 2003) and Th/Yb (Sendjaja and Kimura, 2010), and clay minerals assemblages, i.e., kaolinite/illite ratio (Wan et al., 2010) from this site all exhibit features comparatively close to the average value for the Mekong-derived suspended matter, indicating the dominant terrigenous supply from the Mekong River (Liu et al., 2004). Although the glacial drainage systems on the emerged Sundaland would significantly increase the contribution from the Malaysian Peninsula and Borneo (Fig. 1B), similar clay composition at ODP Site 1143 since about 5.2 Ma with those from the Mekong River indicates the prevailing source of the Mekong River (Wan et al., 2010).

For the relative lower CPI during the Pliocene and most late Quaternary interglacials, four possible factors can be considered: petroleum intermixture, postdepositional alteration, older detrital matter mixing and mixing by marine algae. (1) For petroleum intermixture, the presence of petrogenic hydrocarbons commonly with a CPI approximating 1.0 will reduce the final CPI in sediments, as used to evaluate the oil contamination in some modern sediment (Jeng, 2006; Seki et al., 2006). However, long-term petroleum intermixing since the Pliocene in a marine setting as big as the South China Sea is not rational. (2) For postdepositional alteration, the microbial degradation and diagenesis process often weaken or even eliminate the odd carbon performance in alkanes. Although a greater contribution of the degraded alkanes to the Pliocene lower

CPI values by postdepositional alteration may have been likely, a similar cause seems irrational to explain the similar lower CPI in the later Quaternary interglacials when such alteration is insignificant. Meanwhile, higher alkenone abundance produced by planktonic algae in the Pliocene than that in the Holocene (unpublished data) further indicates very little influence by postdepositional alteration. (3) For older detrital matter intermixture, the older organic matters which had suffered from microbiological deterioration and/or thermal diagenesis will depress the prominence feature of the add carbon number alkanes and reduce the CPI. The lower CPI reflects the mixing by more altered and matured organic matters, with petroleum bearing a CPI value of 1 representing an extreme case. As a consequence, the mixture of the altered matters will moderate the CPI (Shintani et al., 2011; Zhou et al., 2012). Matters in the exposed shelf during glacial low sea level may have undergone similar alteration, and their reposition during the subsequent high sea level will cause a lowered CPI. The enhanced precipitation during Pliocene and Pleistocene interglacials, as discussed below, would also favor erosion and probably re-deposition of the altered matters, consequently resulting in a reduced CPI. Even under this situation, the *n*-alkanes from higher plants were still predominant (Zhou et al., 2012). (4) For marine algal response, as the marine biota synthesize homogeneous *n*-alkanes without carbon preference feature especially for those long chain alkanes ($>C_{24}$), a relative lower terrestrial input due to coastline forward during high sea level periods of the Pliocene (10–20 m higher than today, Raymo et al., 1996) and the Pleistocene interglacials may have counteracted by increasing accumulation of marine-source particles, subsequently resulting in reduced CPI, as revealed in the work of Horikawa et al. (2010) and Kawamura et al. (2003). Similarly, in a core close to our site, the $\delta^{13}C$ of C_{29} and C_{31}-alkane is relatively stable over the past 30 ka, which has led Hu et al. (2003) to consider a major contribution of terrestrial source to the odd carbon alkanes rather than marine source alkanes because the latter will yield a comparatively heavier $\delta^{13}C$. This example indicates that the rising marine source during the Holocene has had little influence on high molecular weight odd carbon alkanes. Thus, we conclude that the increasing altered and re-deposited detrital matters and marine sources to the alkanes have most likely reduced the CPI but their influence on the high molecular weight odd carbons especially their carbon ratio has been minor. In addition, the generally lower CPI values in sediments in low latitude compared to those in mid to high latitude (Ohkouchi et al., 1997; Bendle et al., 2007; Horikawa et al., 2010) may represent the background values in the ambient tropics, and does not necessarily hint any source change. Therefore, the alkane record recovered at ODP Site 1143 can be used as dependable record for paleoclimate interpretation. The positive relation between CPI and chain length index (ACL or C_{31}/C_{27}), as presented here for ODP Site 1143 spanning the Plio-Pleistocene, also occurs in western Africa marginal sediments and western Pacific aerosols (Rommerskirchen et al., 2003; Bendle et al., 2007), implying a hydro-climate linkage with the CPI rather than merely a connection to source, although further researches are needed to quantify the influence of factors including source on the CPI.

4.2. Hydro-climate implications by the alkane record

4.2.1. Glacial–interglacial patterns

The alkanes from ODP Site 1143 at glacials are more abundant with longer-chain members, while alkanes at interglacials are rarer with shorter-chain members enriched, demonstrating a contrast in terrigenous influx during glacial–interglacial cycles. For example, in the Holocene, the Σalkanes were ~120 ng/g, and the C_{31}/C_{27} ratio was ~1.2. For the Last Glacial Maximum (MIS 2), however, the Σalkanes increased to ~680 ng/g, and the C_{31}/C_{27} ratio increased to ~2.6. For earlier periods, the Σalkanes varied mostly between 100 and 300 ng/g during interglacials, compared to 300–>700 ng/g during glacials (Figs. 2 and 3).

The glacial–interglacial differences in the total alkane profile can be attributed mainly to variability in alkane supply due to sea level fluctuations (Pelejero, 2003). As discussed above, the Mekong River is the dominant terrigenous detrital source for the ODP Site 1143. While, during glacial maxima, at sea level lowstands, the site was ~450 km from the Mekong River mouth (Pelejero et al., 1999) and ~500 km from the exposed Sunda Shelf, where the Paleo-Sunda River (or the Molengraaff River) and its vast drainage system (Molengraaff and Weber, 1920) could have acted as another major source area as well as the transport conduit of terrigenous sediments. Dramatic changes in likely varied distance also occurred from the site to the southern coast along the Malay peninsular and Borneo Island. Accordingly, great reductions in distance between the site locality and river mouths enhanced the deposition of alkanes at ODP Site 1143 during glacial periods, especially during the late Pleistocene, as supported by the similar variations between the Σalkanes and the benthic $\delta^{18}O$, a global ice volume proxy (Fig. 2). Meanwhile, strengthened Eastern Asian Winter Monsoon during glacials could have also enhanced eolian input to the glacial alkane deposition. To distinguish fluvial from eolian alkanes deposition in deep-sea sediment cores is difficult, however, although fluvial transportation rather than eolian supply for the most of the modern South China Sea sediments have been demonstrated in previous studies (Wang, 1999; Wang and Li, 2009).

Hot weather, reduced moisture and grassland vegetation will favor the biosynthesis of longer chain length molecular so to adapt to minimal cuticular permeability. The controlling factor depends on regional dominating hydro-climatic features (Kawamura et al., 2003; Rommerskirchen et al., 2003, 2006a,b; Schefuß et al., 2003; Bendle et al., 2007; Cui et al., 2008; Rao et al., 2011). In our study, the longer and shorter chain alkanes represented by C_{31} and C_{27}, respectively, both mimic the Σalkanes record showing high values in glacials and low values in interglacials. As indicated by the C_{31}/C_{27} ratio, however, the relative higher abundance of longer chain alkanes during glacials contradicts a high temperature scenario in the above cited studies, given that the glacial sea surface temperature in the region over the last 1 Ma had dropped as much as 3.3 °C from ~29 °C to 25.7 °C (Fig. 2) (Li et al., 2011). Our results therefore imply that (1) unlike other studies, the warm interglacial did not favor longer chain alkanes onshore of the southern South China Sea, (2) rapid degradation of the relative shorter chain alkane, i.e. C_{27} alkane, (3) a higher amount of longer chain alkanes was transported to the site locality during glacials, (4) variations in the relative inputs from various sources enhanced, (5) reworked particles increased on the exposed shelf during glacial sea level low and (6) moisture or precipitation, rather than temperature alone, has been acting as a decisive factor in the distribution of different chain length alkanes observed at ODP Site 1143.

As alkane chain length in modern plants on land increases with rising temperature (Kawamura et al., 2003; Bendle et al., 2007; Cui et al., 2008), warm interglacials in the Quaternary are expected to have similarly facilitated biosynthesization of longer chain leaf waxes in the surrounding source regions. However, the present increases of alkane chain length during glacials, as presented above for ODP Site 1143, contradict with modern observations. The record of high C_{31}/C_{27} values during glacials could have possibly been caused by the selective biodegradation of the relative shorter chain alkane, i.e. C_{27}-alkane prior to C_{31}-alkane (Buggle et al., 2010). However, this process will favor in warm interglaciations to yield a higher C_{31}/C_{27} than that in cold glaciations, but the observed C_{31}/C_{27} during glaciations indicates a relative weak impact of the selective degradation. Similarly, selective transportation and

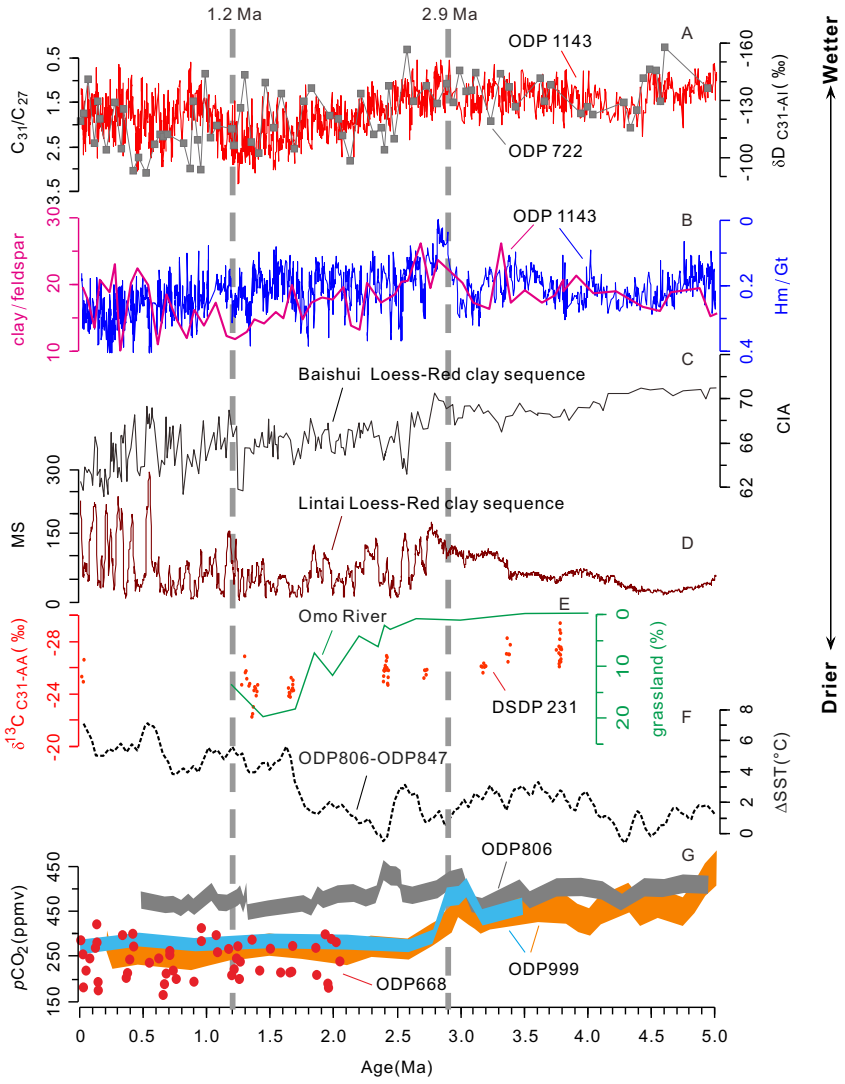

Fig. 4. Paleoclimate records over the past 5 Ma. (A) Ratio of *n*-C_{31} and *n*-C_{27} at ODP Site 1143 (red) and hydrogen isotope ratio of *n*-C_{31} alkane at ODP Site 722 (gray, Huang et al., 2007); (B) Ratios of hematite/goethite (Hm/Gt, blue) and clay/feldspar (pink) at ODP Site 1143 (Wan et al., 2006; Zhang et al., 2009); (C) Chemical index of alteration (CIA) in Baishui loess-red clay sequence (Xiong et al., 2010); (D) Magnetic susceptibility (MS) from Lingtai in Chinese Loess Plateau (An et al., 2001); (E) $\delta^{13}C$ of *n*-C_{31} alkanoic acids from DSDP Site 231 (red dots, Feakins et al., 2005), superimposed with the abundance of taxa indicative of grassland ecosystems in the Omo River in Africa (green line, Bobe and Behrensmeyer, 2004); (F) Zonal temperature variations between tropical eastern and western Pacific: $\Delta SST_{806-847}$ (Wara et al., 2005); (F) pCO_2 estimates at ODP Site 806 (gray band based on alkenones reconstruction, Pagani et al., 2010), ODP Site 999 (orange band based on alkenones reconstruction and blue band based on boron derivation, Seki et al., 2010) and ODP Site 668 (red dots based on boron derivation, Hönisch et al., 2009). Vertical dashed lines mark major hydrological events at 1.2 Ma and at 2.9 Ma, respectively. (For interpretation of the references to color in this figure legend, the reader is referred to the web version of this article.)

deposing of contemporary longer C_{31}-alkanes during glacials seems unlikely. In general, alkanes are synthesized more or less synchronously in the plant wax before being transported, and their common chemical features owing to the close carbon numbers make them have similar transport efficiency and high resistance to selective biodegradation, transport, and deposition (Poynter and Eglinton, 1990). The increases in longer chain alkanes during glacials at the site, therefore, contradict with modern observations. If the increasing accumulation of the longer chain length alkane (high C_{31}/C_{27}) was only due to dramatically enhanced glacial alkanes input from the exposed Sunda Shelf at the late Quaternary glacial sea level lows, a similar C_{31}/C_{27} trend would be expected also for the Σalkanes. Our results shown in Fig. 2, however, do not support the increased glacial input mechanism. As the main vegetation type in SE Asian subcontinent has always been tropical rainforest, its expansion on to the exposed Sunda Shelf would result in a constant alkane index regardless of the amount of the alkane input during the glacials. Although the exposed Sunda Shelf may shed some older shelf sediment into the deep sea (Hu et al., 2012), their relative lower C_{31}/C_{27} as from an interglacial source would have reduced the glacial C_{31}/C_{27} rather than increased the ratio. Meanwhile, the alkanes derived from reworked continental shelf are one-off action and, consequently, are limited components compared with those from the overlying vegetations. But none of these seems tenable to answer convincingly why the C_{31}/C_{27} was high during glacials at ODP Site 1143.

The glacial hydrological change in the region was marked by reduced humidity, as indicated by modeling and by many geological records (An et al., 2001; De Deckker et al., 2002; Wang and Li, 2009). Climate conditions with reduced humility often favor the production of longer alkanes (Dodd and Afzal-Rafii, 2000; Rommerskirchen et al., 2003, 2006a,b; Schefuß et al., 2003; Rao et al., 2011). As the ice volume proxy—the benthic oxygen isotope has remained relatively stable for almost all the interglacial periods since the late Pliocene, a similarly stable state can be expected for vegetation source variability due to little geography change in

warm periods. Combined with the relative steady temperature, the possibility for the remarkable increasing of C_{31}/C_{27} from 0.6 in the late Pliocene to 2 in the mid-Pleistocene at ~1.2 Ma during the interglacial warm periods can only contribute to changes in hydroclimate conditions. Thus, the alkane chain length record at ODP Site 1143 well preserved the information of climate variability more than the source change or other factors. As moisture plays a crucial role on alkane biosynthesis in the climate system (Schefuß et al., 2003; Calvo et al., 2004; Horikawa et al., 2010), a relative high humidity could have been likely the key to facilitating the relative shorter chain alkanes during interglacials, i.e. more C_{27}- than C_{31}-alkane production regardless of vegetation species.

In Figs. 3 and 4, we compared our alkane record (C_{31}/C_{27}) with various monsoon precipitation and other climate proxies: Hematite/Goethite (Hm/Gt) ratio and clay/feldspar ratio from ODP Site 1143 (Wan et al., 2006; Zhang et al., 2009), magnetic susceptibility and chemical index of alteration in loess-red clay sequence (An et al., 2001, 2005; Xiong et al., 2010), δD of *n*-C_{31} alkane from ODP Site 722 (Huang et al., 2007), $\delta^{13}C$ of *n*-C_{31} aliphatic acid from DSDP Site 231 (Feakins et al., 2005), grassland indicator data from Africa (Bobe and Behrensmeyer, 2004), estimated *p*CO2 from ODP Site 806, west Pacific (Pagani et al., 2010; Seki et al., 2010). Parallel changes between C_{31}/C_{27} and these records in most intervals may justify its use as a precipitation index, as detailed below.

The terrestrial alkanes found in ODP Site 1143 sediments are originated from the south Asia continent, where the annual temperature is constantly high, without great summer and winter seasonal difference but only rainy and dry seasons. The controlling factor on the variability of the chain length in the local plant wax is likely moisture or precipitation but not temperature although whether there was a temperature threshold over glacial–interglacial transitions is not clear. Therefore, the relative high C_{31}/C_{27} values over glacials may correspond to drier conditions with lesser rainfalls, and the lower C_{31}/C_{27} values over interglacials to wetter conditions with stronger rainfalls, as depicted previously by Brincat et al. (2000). Drier conditions over glacial periods in South China are also characterized by increases in herb pollen abundance at ODP Site 1144 from the northern South China Sea because herb vegetation prefer dryer conditions (Fig. 3E) (Sun et al., 2003).

For hydrological conditions during the last glaciation in southern Asia, high C_{31}/C_{27} values from our work imply a decrease in humidity, although the southern South China Sea like other parts of the western Pacific warm pool had experienced high temperature, strong evaporation and heavy rainfall for most of time. The predominating vegetation along the southern coastal areas of the southern South China Sea was rainforests, by a C_3 photosynthetic mechanism, even in glacials (Sun et al., 2000; Hu et al., 2003; Wang et al., 2009). This ecosystem possibly can be traced back to the Pliocene, when the overall hydrological and geological framework in this area started to be stabilized. Accordingly, the climate-induced change in carbon fixation pathway, as reflected by the C isotope of the leaf waxes, may not have occurred in this area, so that $\delta^{13}C$ values of higher plants *n*-alkanes alone may not reflect the climate change reality (Hu et al., 2003). Comparatively, however, higher plants molecules distribution can provide more meaningful information. Although rainforest remained abundant during the glacials in SE Asia, evidence from the ratio of the dry/humid phytoliths in sediments from the southern South China Sea and other western Pacific localities indicates relatively drier conditions during the last glaciation (Wang et al., 2009; Bian et al., 2011). Expansion of open savanna-woodland vegetation in glacial SE Asia also indicates a moisture reduced environment (Bird et al., 2005). Reducing precipitation during the last glaciation, however, may not necessarily lead to the grassland establishment and other major vegetation type changes in a region prevailed by extremely warm and humid climate like SE Asia (Anshari et al., 2004; Bird et al., 2005; Wang et al., 2009). As shown in Fig. 5, the precipitation proxy C_{31}/C_{27} from the southern South China Sea and the Indian summer monsoon index from South China (An et al., 2011) both show humidity and summer monsoon beginning to enhance in interglacial intervals. Compared to C_{31}/C_{27} and palynological records, however, the $\delta^{13}C$ of plant alkanes appears to be less sensitive to climate change in regions without C_4-type vegetation, as revealed in studies of Lake Baikal and South China Sea sediments (Brincat et al., 2000; Hu et al., 2003). Along the western African coast, however, a positive correlation exists between increasing chain length wax with enhanced C_4 vegetation, enriched alkane $\delta^{13}C$ and intensified aridity (Rommerskirchen et al., 2003; Schefuß et al., 2003).

4.2.2. Longer term patterns

Similar to the glacial–interglacial alkane record, the long-term alkane patterns show low Σalkanes and low C_{31}/C_{27} values in warmer periods, particularly for the early to mid-Pliocene warm period before 2.7 Ma. As in foregoing discussion, low Σalkanes and low C_{31}/C_{27} values correspond to higher sea level and wetter hydroclimate conditions. Conversely, the stepwise increases in Σalkanes and C_{31}/C_{27} values in the late Pliocene and mid Pleistocene, especially for alkane ratio after 2.9 Ma and for alkane accumulation since 1.2 Ma, are considered to have been affected by drier conditions and low sea level during glacial cooling. Based on the C_{31}/C_{27} as a precipitation proxy, therefore, the long term alkane trends imply three periods of hydro-climate changes in the region: (1) humid climate conditions during the early to mid-Pliocene (5.0–2.9 Ma); (2) reduced precipitation during 2.9–1.2 Ma; and (3) big fluctuations since 1.2 Ma.

(1) Humid climate conditions during the early to mid-Pliocene (5.0–2.9 Ma)

During early to mid-Pliocene, the C_{31}/C_{27} ratio varied between 0.7 and 2.1, averaging ~1.4, or by ~0.4 lower than the late Pleistocene average. The ratio for the early Pliocene interval of 5.0–4.4 Ma reduced to an average of 1.15. Although increasing slightly at 4.4–4.2 Ma, the overall low C_{31}/C_{27} values for this early to mid-Pliocene period indicate humid hydro-climate conditions probably associating also with a high sea level.

Consistent with the alkane record, the formation of iron oxide minerals, especially the lower hematite%, and the increase trend of kaolinite/illite ratio at the same site are all related to enhancing of chemical weathering likely caused by increased humidity intensity in the early Pliocene (Zhang et al., 2009; Wan et al., 2010). Relative humid conditions prevailed not only in South Asia but also in North Asia, as humidity-sensitive arbores increasing in the Loess Plateau and extremely mature soils and high Fe_2O_3 ratios in the loess-red clay sequence were all created under warm and wet climate (Ding et al., 2001; Wan et al., 2006). Thermo-humidiphilous terrestrial mollusks predominated in the early Pliocene fossil assemblage in the western Chinese Loess Plateau, also indicating the prevalence of warm, moist conditions driven by strong summer monsoon during this time interval (Wu et al., 2006; Li and Wu, 2010). These regional records were part of the global picture for the early to mid-Pliocene when the global temperature was about 3 °C higher than present (Ravelo et al., 2004) and warm ocean waters supplied abundant atmospheric moisture for precipitation on the continents (Zachos et al., 2001).

The highly humid Pliocene climate was truncated by a relative arid interval during 4.5–4.2 Ma, as evidenced by an increase of the average C_{31}/C_{27} ratio from 1.0 to 1.5 and a decrease in the Σalkanes, accompanied also by a positive shift in foraminiferal oxygen

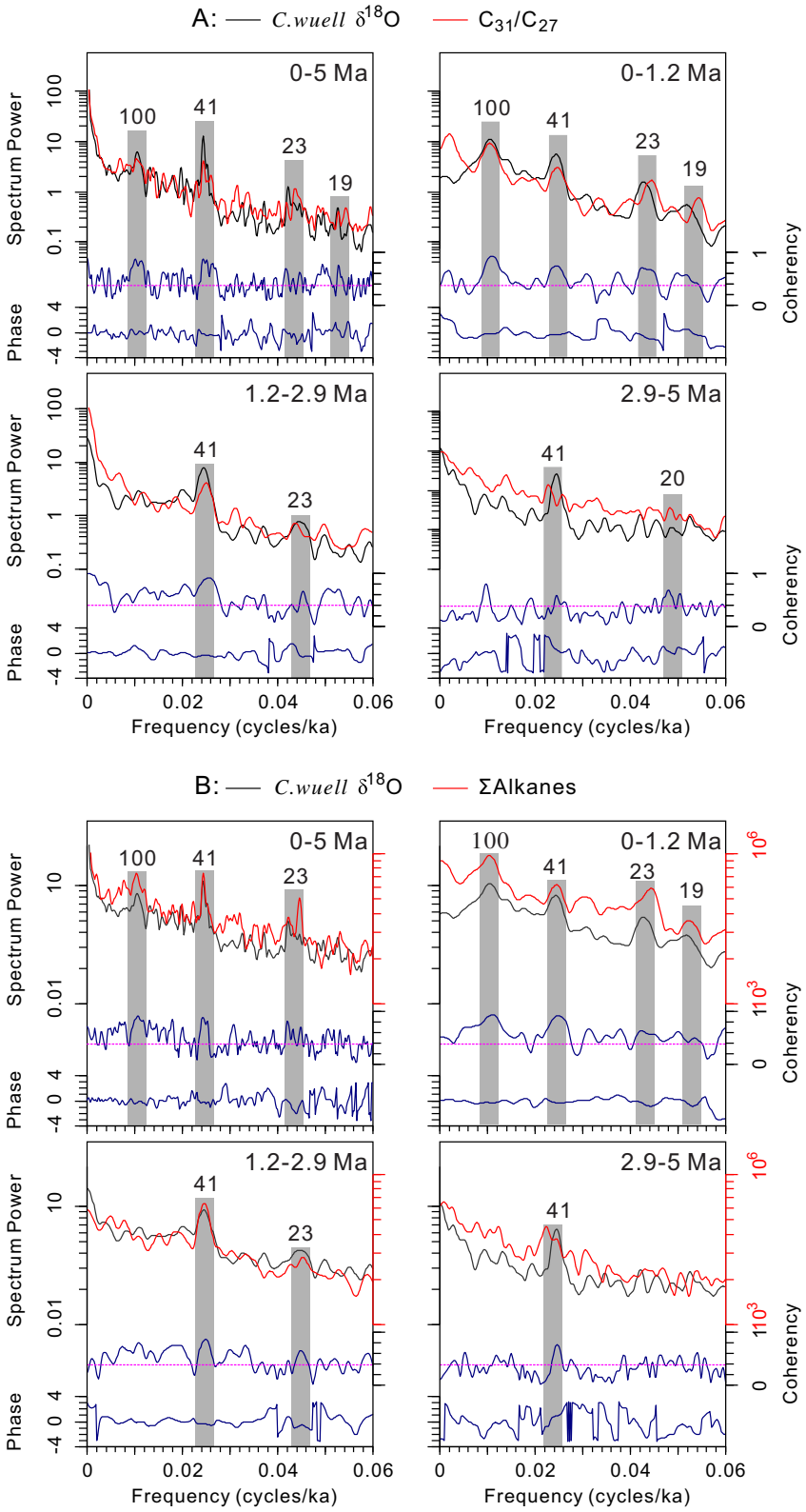

Fig. 5. Cross Blackman–Tuckey spectrum of benthic $\delta^{18}O$ with C_{31}/C_{27} ratio (A) and Σalkanes (B) at ODP Site 1143 for the past 5 Ma using the Analyseries software package (Paillard et al., 1996). Spectral densities are plotted on log scales. The horizontal dashed lines (pink) indicate confidence at the 90% level in the coherence spectra. Periods of the main spectral peaks above the 90% confidence level are labeled. (For interpretation of the references to color in this figure legend, the reader is referred to the web version of this article.)

isotopes (Fig. 2). Reduced precipitation inferred for this period is consistent with other proxy results, such as terrestrial snail fossil assemblages, decreased pedogenesis in red clay sequences, prominent coarsening trend in dust grain size, reduced chemical weathering and higher Hm/Gt values (Rea et al., 1998; Sun et al., 2006; Wu et al., 2006; Clift et al., 2008; Zhang et al., 2009).

From 3 to 2.9 Ma, the C_{31}/C_{27} ratio decreased rapidly from 1.98 to 0.55, approaching the lowest value for the past 5 Ma, likely

corresponding to a period with strong rainfall. From 4.2 to 2.7 Ma, significant increases in the difference between benthic and planktonic faunal $\delta^{18}O$ ($\Delta\ \delta^{18}$Ob-p) have been attributed to enhanced monsoon precipitation that diluted the surface seawater with relatively ^{18}O-depleted rainwater (Tian et al., 2004). Mineralogical results, including decreases in Hm/Gt, increases in the weight percent of clay minerals and high values of the Fe_2O_3, also imply an intensified East Asian summer monsoon and stronger rainfall at this time (Ding et al., 2001; Wan et al., 2006; Zhang et al., 2009). Other evidence of intensified summer precipitation includes the increasing magnetic susceptibility and chemical alteration in loess-paleosol-red clay sequence and the stacked summer monsoon index based on magnetic susceptibility and carbonate abundance (Sun et al., 2006, 2010; Xiong et al., 2010). Similarly, the significant carbon isotopic enrichment in pedogenic carbonates at ~2.9 Ma indicating a distinct C_4 plant expansion period in Chinese Loess Plateau, has been considered to be correlated with the strengthened East Asian summer monsoon circulation, because C_4 grasses in the semiarid monsoonal region of East Asia are associated with warm and wet conditions, not with the dry condition as in Africa (An et al., 2005; Zhang et al., 2006).

(2) Gradually reduced precipitation after the onset of Northern Hemisphere Glaciation (2.9–1.2 Ma)

Since ~2.9 Ma, the C_{31}/C_{27} ratio increased stepwise (Figs. 2 and 3), indicating reduced precipitation in response to global cooling and ice sheet expansion on high latitudes. Reduced precipitation during this period was also recorded by other monsoon proxies, including increases in Hm/Gt values and decreases in the clay/feldspar ratio, magnetic susceptibility and the loess-paleosol carbonate $\delta^{13}C$ (An et al., 2005; Sun et al., 2006; Wan et al., 2006; Zhang et al., 2009), in a time of substantial weakening of the Eastern Asian Summer Monsoon associated with the strengthened glaciations (An et al., 2001). Higher leaf wax δD values in Arabian Sea sediments also imply reduction of precipitation in the source region during this period (Huang et al., 2007).

Compared to earlier intervals, the Σalkanes and C_{31}/C_{27} from this period show more obvious glacial–interglacial fluctuations, as seen in C_{31}/C_{27} increases from 1.7 to 3.3 in glacials and from 0.5 to 1.9 in interglacials, very similar to the contemporary benthic $\delta^{18}O$ fluctuations. These results demonstrate a teleconnection between global ice volume waxing and waning and the regional wet and dry conditions modulated by monsoon climate.

At ~1.4–1.2 Ma, the C_{31}/C_{27} ratio reached a maximum value of ~2.5 (Fig. 3). Together with the record of the iron oxide minerals and mineral assemblage (Wan et al., 2006; Zhang et al., 2009), this C_{31}/C_{27} maximum indicates an arid interval. Increased aridity associating with weakening summer monsoon over Asia at this time has been documented by low magnetic susceptibility in loess deposits and by a retreat of the C_4 plants (An et al., 2005). Reduced precipitation or increased aridity at this period appears to be a large scale phenomenon, as reported also from localities including the Indian Ocean with low sediment flux (Rea, 1992) and Lake Bungunnia of southern Australia with abundant aeolo-lacustrine quartz silts (McLaren and Wallace, 2010). Meanwhile, the contemporary C_4 grass expansion in Africa is also largely a result of a local facies shift to arid environments (Levin et al., 2004; deMenocal, 2004, 2011; Feakins et al., 2005).

(3) Big fluctuations since the Mid-Pleistocene Transition (1.2 Ma–present)

Since ~1.2 Ma, strong fluctuations between 3.5 and 0.4 in the C_{31}/C_{27} ratio indicate the alternation of dry and wet hydro-climate conditions in response to modern glacial–interglacial oscillations first established about 0.9–1.2 Ma ago during the mid-Pleistocene climate transition. The return of wet conditions since 1.0 Ma was possibly due to ephemeral strengthening of summer monsoon (Jiang and Ding, 2008). A relative humid climate condition during this period is also recorded by increased clay/feldspar in the same core, as well as depleted leaf wax δD values from the Arabian Sea (Huang et al., 2007) and a major lake phase in the low latitude East Africa (Trauth et al., 2005, 2007), pointing to a similar moisture history between Asia and Africa. However, this is not supported by iron oxide minerals (Fig. 4), which with increased Hm/Gt indicate low humidity continuing from 0.9 Ma without any obvious moistening events (Zhang et al., 2009). Probably, in addition to the simple dry-glacial and wet-interglacial forcing, factors such as hydroclimate changes over the northern Australia and over the western Pacific may have some joint impact on the C_{31}/C_{27} profile of the southern South China Sea over the last 1.2 Ma.

The amplitude of C_{31}/C_{27} fluctuations after 0.4 Ma is 1.2 on average (Fig. 4), compared to 1.7 during 0.4–1 Ma, and this relative low amplitude is consistent with Indian summer monsoon variability (An et al., 2011). Our southern South China Sea alkane record with higher C_{31}/C_{27} values in glacials indicates more arid conditions in glacials than interglacials, while the integrated Indian summer monsoon index with higher values in interglacials implies more moisture due to stronger summer monsoon in interglacials. Thus, both results support the common belief that increases in high latitude ice sheet are companied with reduced rainfall in low latitudes.

4.3. Typical tropical hydrological dynamics events

4.3.1. Hydrological change before the extensive Northern Hemisphere Glaciation

Although significant Northern Hemisphere Glaciation beginning ~2.75 Ma ago has been known for ages, the forcing mechanism for this extraordinary climate event is still unsolved. Our alkane results, particularly the C_{31}/C_{27} variations, indicate strengthened precipitation before the full onset of northern hemisphere glaciation, a trend since 4 Ma and becoming stronger during 3–2.8 Ma even excess the Holocene intensity. Considering the warm climate during this period, the increasing moisture in low latitude regions during 3–2.8 Ma would have accelerated evaporation of surface water and its poleward transport into high latitudes, and the accumulation of the transported moisture may ultimately have played a key role in the high latitude ice sheet growth (Raymo and Nisancioglu, 2003; Fedorov et al., 2006).

The closure of the mid-American seaway and Indonesian seaway at ~4 Ma changed the equatorial circulation patterns over and across oceans (Haug and Tiedemann, 1998; Chaisson and Ravelo, 2000; Cane and Molnar, 2001). The formation of the Panamanian isthmus restricted the surface-water exchange between the tropical Atlantic and Pacific and led toward the development of the modern east-west gradient in surface hydrography of the Pacific. As a consequence, it may have also caused new ocean–atmosphere feedback mechanisms and/or changes in air-sea interaction that modified tropical winds (Chaisson and Ravelo, 2000; Haug and Tiedemann, 1998). Tectonically driven closure of the seaway would lead to increasing precipitation in northern high latitude as simulated using the coupled atmosphere-ocean general circulation model (Lunt et al., 2008). In addition, further uplift and expansion of the northern and eastern Tibetan Plateau around 4.5–2.6 Ma changed the circulation over Asian continent, resulting in the strengthening of both the summer and winter monsoons of the Pliocene (Zheng et al., 2000, 2004; An et al., 2001). Increased precipitation in the loess plateau had been simulated with plateau

extension along its eastern and northern margins in a climate-model experiment through the alteration of thermally forced circulation (An et al., 2001). The growing of the Tibetan Plateau seemed to affect precipitation in eastern China through atmospheric dynamics associated with its perturbation to the mid-latitude jet (jet stream) (Molnar et al., 2010).

The variation trend of our alkane derived hydro-climate record is also shared by atmospheric CO_2, a key factor in the Cenozoic climate change, with a rapid increase of more than 100 ppmv to near the maximum value at ~3 Ma (Fig. 4G, Pagani et al., 2010; Seki et al., 2010). These parallel changes between two independent climate proxies cannot be merely coincident but manifest their close relationship. Probably, high pCO_2, accompanying high temperature, had promoted higher moisture accumulation in the high latitude, providing a favorable precondition for subsequent ice buildup during the great reduction in boreal insolation at ~2.7 Ma. On the other hand, increased monsoonal precipitation may in turn have induced strengthened chemical weathering and continental erosion, consequently decreased the atmospheric pCO_2 over a threshold, and finally triggered the onset of extensive northern hemisphere glaciation (Lunt et al., 2008).

Similarly, the almost parallel changes between the ice sheet proxy (benthic $\delta^{18}O$) and the precipitation proxy (C_{31}/C_{27}) continued until 2.7 Ma when the two proxies began to increase their variations sometimes even to different directions (Fig. 2G), indicating a hydro-climate shift from the relative stable warm and wet Pliocene to an unstable cool and dry Pleistocene. Along with the NHG, ocean evaporation weakened and precipitation reduced globally as implied by our southern South China Sea alkane record and other precipitation proxies (Fig. 4). As more and more moisture was locked in high latitude ice, global aridification after 2.7 Ma promoted grassland expansion in Africa (deMenocal, 2004).

4.3.2. Hydrological change before the Mid-Pleistocene transition

Beside the puzzle of the initial northern hemisphere glaciation, the dominant global climate periodicity change from the 40 ka obliquity cycle to the 100 ka eccentricity cycle at 1.2–0.9 Ma during the mid-Pleistocene transition (MPT) is also an enigma. Immediately prior to ~1.2 Ma, a period of strong aridity in SE Asia is recorded in our C_{31}/C_{27} ratio (Fig. 2), which is consistent with the positive shift of soil carbonate $\delta^{13}C$ in eastern Africa (Levin et al., 2004), remarkable coarsening events in the quartz mean grain size in Chinese loess records (Sun et al., 2010), and dramatically increasing of dust supply to the Southern Ocean (Martínez-Garcia et al., 2011), as well as strong variability in the India-Asian monsoon during this time interval (Clemens et al., 2008; Sun et al., 2010). This long term shrink in precipitation was ended at ~1.2 Ma, followed by a period of remarkable decline in C_{31}/C_{27} from 3.3 to 0.6 between 1.2 and 1 Ma in responding to climatic transition from dry to wet conditions over the tropical East Asia (Fig. 4A). Several large scale phenomena were either related to or concurred with this pre-MPT climate change. (1) The east-west equatorial Pacific temperature gradient started to increase (Wara et al., 2005). As modeling suggests, the termination of a permanent El Niño state in the Pliocene may have increased precipitation even in high latitudes (Lunt et al., 2008). With the strengthening of the Walker circulation, warm water gradually piled-up in the western Pacific not only promoted moisture accumulation but also a quick change from the long term reduced precipitation to enhanced precipitation with large fluctuations. Therefore, enhanced moisture in low latitudes would at least partly account for the fully development of ice sheets since ~1.2 Ma (Liu and Ding, 1993; Raymo et al., 2006). (2) A retreat of nutrient-rich water sourced from the high latitude ended the late Pliocene/early Pleistocene productivity maximum in the eastern equatorial Pacific (Lawrence et al., 2006). However, the mechanism about how the reconfigured water masses in high latitudes influenced the low latitude hydrological climate is not clear (Marlow et al., 2000; Lawrence et al., 2006). The obscurity of the 400-ka long eccentricity cycle in the deep ocean $\delta^{13}C$ maxima since ~1.6 Ma may have also associated with restructuring of the ocean water (Wang et al., 2010). (3) A slight increase in pCO_2 by ~50 ppmv at 1.2–1.0 Ma (Fig. 4G, Hönisch et al., 2009; Pagani et al., 2010) was probably repeating the situation at ~3 Ma in associating with increasing moisture (Lunt et al., 2008), although at a much small scale.

Integrating these regional phenomena into a global context, therefore, may help unveil the cause of this major shift in climate and improve our understanding of climate change over the entire Pliocene-Pleistocene at large (McLaren and Wallace, 2010). The pre-MPT climate shift corresponding to a pCO_2 variation reinforces the important role of CO_2 to hydrological processes, especially precipitation, evaporation and moisture supply, as falling CO_2 will reduce low latitude rainfall, and vice versa (Liu, 2011). However, this pre-

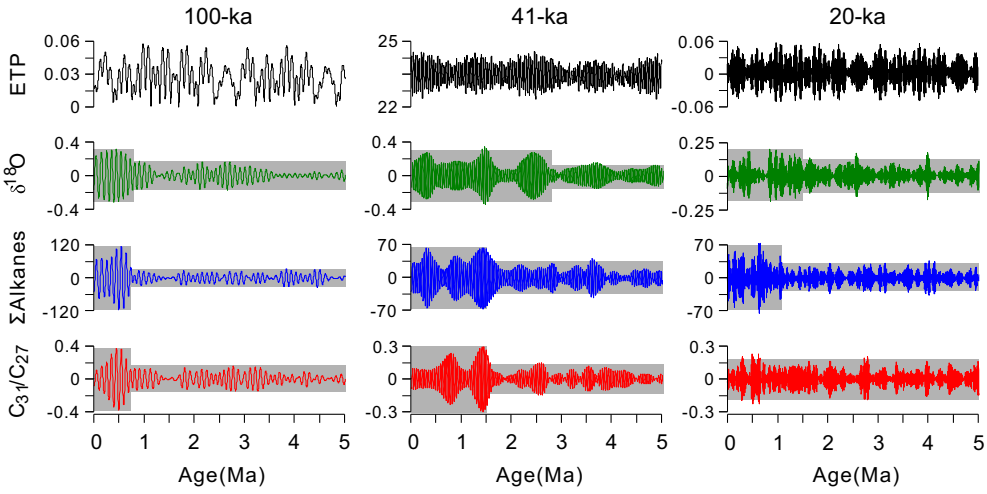

Fig. 6. Comparison of the filtering results on the 100-, 41-, 20-ka bands by the Analyseries software package (Paillard et al., 1996) for ETP with benthic foraminifer *Cibicidoides wuellerstorfi* $\delta^{18}O$, Σalkanes, and C_{31}/C_{27} at ODP Site 1143. Astronomical target curve (ETP) was based on the sum of the normalized eccentricity (*e*), obliquity (*t*) and precession (*p*) time series of the La2004 solution in the ratio 1:1:−1 (Laskar et al., 2004). Gray bars denote the amplitude of filtered components of different parameters at the three orbital bands.

MPT pCO_2 increase may have been too weak to fully account for the notable C_{31}/C_{27} drop over the same period. If aridity increase was responding to the onset of Northern Hemisphere Glaciation, the pre-MPT termination of a longer term aridity enhancement at ~1.2 Ma has to be the combined result of a strengthened Walker circulation, reconfigured water mass and further enhanced global pCO_2. After that time the global climate shifted from the higher frequency, lower amplitude trait in the early Pleistocene to the lower frequency, higher amplitude feature in the middle and late Pleistocene (Ravelo et al., 2004), as documented also in the South China Sea $\delta^{18}O$ and alkane records (Figs. 2 and 5).

4.4. Hydro-climate linkage between low and high latitudes

The glacial–interglacial cycles of the past 3 Ma represent some of the largest and most studied climate variations of the past, and the physical mechanisms driving these cycles are now well understood, i.e., orbital forcing (Raymo et al., 2006). As shown in Fig. 5, cross-spectral results provide further evidence of a teleconnection between ice volume, low latitude terrestrial input and hydro-climate variability for the past 5 Ma. In general, these parameters all exhibit the dominant peaks around the primary orbital cycles (eccentricity, obliquity and precession) but show respective features in three intervals: 5–2.9 Ma, 2.9–1.2 Ma and 1.2 Ma–present. Over the past 1.2 Ma, the Σalkanes and C_{31}/C_{27} are both strongly coherent with the benthic $\delta^{18}O$, a global ice volume and sea level proxy, and almost in-phase at 100-, 41- and 23-ka orbital periods. During the interval 2.9–1.2 Ma, the Σalkanes and C_{31}/C_{27} show distinct peaks, high coherency, and a near-zero phase relationship with $\delta^{18}O$ at the 41-ka band, but a weak peak and low coherency at the 100-ka band and a quick change in phase at the 23-ka band. Prior to 2.9 Ma, both alkane parameters and the benthic $\delta^{18}O$ display only a strong 41-ka obliquity cycle (Fig. 5). The 41-ka band remain strong throughout the entire sections and the coherency at this band is high during every time intervals indicating that this component is the dominant cycle for terrestrial deposition, precipitation variability and ice volume change. The eccentricity component becoming prominent for the three parameters with a highly coherency only after 1.2 Ma reflects the mid-Pleistocene transition, when the earth's climate turned into a dominant 100-ka regime as indicated by the filtered results (Fig. 6). The precession signal became stronger since 2.9 Ma, although it occurred with weak amplitude prior to 2.9 Ma in the C_{31}/C_{27} record.

Although the cause of northern hemisphere glaciation as relating to the low-high latitude interaction is still unresolved, the important role of the low latitude process cannot be ignored. As the low latitude vegetation and precipitation evidence, the South China Sea Σalkanes and C_{31}/C_{27} records provide critical information on the low-high latitude linkage. In Fig. 2G, whereas the Σalkanes exhibits large stepwise increases in amplitude variations after ~1.2 Ma, the C_{31}/C_{27} maintains a gradual to low amplitude increasing trend as early as from 5 Ma except a quick jump at ~4.6–4.5 Ma. Before 2.9 Ma, the Σalkanes and the C_{31}/C_{27} are both basically coherent with the benthic $\delta^{18}O$. After 2.9 Ma, the Σalkanes and the benthic $\delta^{18}O$ are coherent, but the C_{31}/C_{27} shows slightly earlier variations than the benthic $\delta^{18}O$. Specifically, the variance of C_{31}/C_{27} began to reduce at 2.9 Ma, while the benthic $\delta^{18}O$ reduced at 2.7 Ma; then C_{31}/C_{27} became to increase at 2.2 Ma, while the benthic $\delta^{18}O$ increased at 2 Ma. However, the subsequent decrease in $\delta^{18}O$ variance occurred earlier at 1.6 Ma than the C_{31}/C_{27} at 1.2 Ma, followed by a major increase in benthic $\delta^{18}O$ variance at 1.2 Ma compared to the C_{31}/C_{27} increase at 1.0 Ma. Since the lower C_{31}/C_{27} values before 2.9 Ma have been attributed to warm and wet hydro-climate conditions, the higher C_{31}/C_{27} values after 2.9 Ma coupled with strong variations slightly earlier than benthic $\delta^{18}O$ changes may indicate a lead of the tropical (or Southern Hemisphere) dynamics including monsoon precipitation over ice volume variability on a long time scale (Fig. 5). As related mainly to late Quaternary sea level variations, the Σalkanes variations follow the global ice volume index $\delta^{18}O$ nicely, with higher Σalkanes values corresponding to increased ice volume (or low sea level). The similar variations between Σalkanes and C_{31}/C_{27} records especially prior to ~2 Ma (Fig. 2G) imply profound effects of precipitation on alkane deposition. Since ~1 Ma, however, Σalkanes, C_{31}/C_{27} and benthic $\delta^{18}O$ all show similar variations between them as influenced more intensively by insolation-driven modulation. Particularly, the C_{31}/C_{27} variance departing from the other two at ~1.2 Ma and after ~0.5 Ma (Fig. 2G) may have resulted from global events of aridity and glacial low sea level, coupled with the development of large scale drainage systems on the exposed Sunda Shelf (Hanebuth and Stattegger, 2004).

The filtered components indicate increased amplitude of the 100-ka periodicity for the $\delta^{18}O$, Σalkanes and C_{31}/C_{27} records since around 0.6 Ma, representing a major shift at the completion of the mid-Pleistocene climate transition from the dominance of the 41- and 20-ka periodicities in earlier intervals (Fig. 6). The filtered 41-ka component show enlarged fluctuations as early as ~2.7 Ma for the $\delta^{18}O$, but delayed to after 2 Ma for the two alkane records. The similar strength in the three orbital elements deduced from the ETP analysis for the last 5 Ma may indicate the driving role of the global ice volume on the terrestrial deposition and precipitation in the tropics, especially over the eccentricity and obliquity orbital cycles. However, the 20-ka component varied within a range during the entire Plio-Pleistocene for the C_{31}/C_{27}, and its variations became stronger since 1.5 Ma for the $\delta^{18}O$ and since 1.2 Ma for the Σalkanes, respectively, suggesting less influence of ice volume on the tropical hydrological dynamics over the precession cycle. The relatively stable 20-ka component on the precipitation index may have accounted for the long term change of C_{31}/C_{27} slightly earlier than the $\delta^{18}O$ and Σalkanes (Fig. 2G). Thus, although the low latitude terrigenous deposition displays a general response to the high latitude ice volume change, the alkane-derived precipitation record reveals a rather complex relationship between the high and low latitude hydrodynamics. Actually, in addition to the general increased ice volume, increased terrigenous deposition and weak precipitation during glacial stages and vice versa during the interglacials, the alkane chain length index reveals more fluctuations than that in the $\delta^{18}O$ over glacial/interglacial cycles as shown in Fig. 3, indicating the low latitude hydrologic process is more complex than the simple waxing and waning rhythms of the global ice volume in high latitudes.

5. Conclusions

High resolution long chain *n*-alkane records from ODP Site 1143 in the southern South China Sea provide meaningful information on hydro-climate change in southeastern Asia over the past 5 Ma. The concentration of these terrigenous waxes (Σalkanes) was relatively low until the mid-Pleistocene when stronger fluctuations between higher values in glacials and lower values in interglacials enhanced. The chain lengths index (C_{31}/C_{27}) is interpreted as responding primarily to humidity change in the tropical western Pacific, with higher ratio values indicating relative drier conditions and lower values comparative wetter conditions. The C_{31}/C_{27} was low before 2.9 Ma, increased between 2.9 Ma and 1.2 Ma and fluctuated widely after 1.2 Ma, implying a long term trend from high humidity in the Pliocene to relative aridity in the mid-Pleistocene, and finally frequent fluctuations between wet and dry conditions since then. Combined with the multi-proxy records, our results demonstrate two distinct high humidity events before

the extensive Northern Hemisphere Glaciation and the mid-Pleistocene transition in the low latitude western Pacific, respectively, as resulting from the tectonic seaway closure plus Tibetan Plateau uplift, and strengthened Walker circulations over the equatorial Pacific, as well as increases in ambient pCO_2. The accumulation of moisture in the low latitude region at ~2.9 Ma may have enhanced weathering, lowered the atmospheric CO_2 and, finally, helped to trigger the glaciation at 2.7 Ma, lending support to previous modeling simulation. The increasing dry hydro-climate conditions since 2.7 Ma in the region correspond to stepwise increases in global cooling and ice volume, and probably also to strengthened Hadley circulations, or monsoon circulations, in the region. The stronger wet/dry fluctuations since ~1.2 Ma are the results of climate oscillations driven by a change of the dominant orbital cyclicity from 40-ka to 100-ka, as well as monsoon dynamics and sea level fluctuations associating with glacial–interglacial cycles. The statistic analysis indicated the driving role of high latitude ice volume over the eccentricity and obliquity orbital cycles, but the low latitude precipitation on the precession component has been more critical. Therefore, we conclude that large-scale hydrological dynamics in the tropical region have contributed greatly to influencing late Cenozoic climate change.

Acknowledgments

We thank Ocean Drilling Program (ODP) for providing the samples. ODP is sponsored by the US National Science Foundation (NSF) and participating countries under management of Joint Oceanographic Institutions (JOI), Inc. Funding for this research was provided by grants from the Ministry of Science and Technology of China (2013CB955704) and the National Natural Science Foundation of China (91228203, 41023004, 41076017 and 40976022), and the China Geological Survey (Project H[2010]MA03-06-04). This research was also supported by Innovation Program of Shanghai Municipal Education Commission (12ZZ031).

Appendix A. Supplementary data

Supplementary data related to this article can be found at http://dx.doi.org/10.1016/j.quascirev.2013.08.007.

References

An, Z.S., Clemens, S.C., Shen, J., Qiang, X.K., Jin, Z.D., Sun, Y.B., Prell, W.L., Luo, J.J., Wang, S.M., Xu, H., Cai, Y.J., Zhou, W.J., Liu, X.D., Liu, W.G., Shi, Z.G., Yan, L.B., Xiao, X.Y., Chang, H., Wu, F., Ai, L., Lu, F.Y., 2011. Glacial–interglacial Indian Summer Monsoon dynamics. Science 333, 719–723.

An, Z.S., Huang, Y.S., Liu, W.G., Guo, Z.T., Clemens, S., Li, L., Prell, W.L., Ning, Y.F., Cai, Y.J., Zhou, W.J., Lin, B.H., Zhang, Q.L., Cao, Y.N., Qiang, X.K., Chang, H., Wu, Z.K., 2005. Multiple expansions of C-4 plant biomass in East Asia since 7 Ma coupled with strengthened monsoon circulation. Geology 33, 705–708.

An, Z.S., Kutzbach, J.E., Prell, W.L., Porter, S.C., 2001. Evolution of Asian monsoons and phased uplift of the Himalaya–Tibetan plateau since late Miocene times. Nature 411, 62–66.

Anshari, G., Kershaw, A.P., van der Kaars, S., Jacobsen, G., 2004. Environmental change and peatland forest dynamics in the Lake Sentarum area, West Kalimantan, Indonesia. J. Quat. Sci. 19, 637–655.

Bendle, J., Kawamura, K., Yamazaki, K., Niwai, T., 2007. Latitudinal distribution of terrestrial lipid biomarkers and *n*-alkane compound-specific stable carbon isotope ratios in the atmosphere over the western Pacific and Southern Ocean. Geochim. Cosmochim. Acta 71, 5934–5955.

Bian, Y.P., Jian, Z.M., Weng, C.Y., Kuhnt, W., Bolliet, T., Holbourn, A., 2011. A palynological and palaeoclimatological record from the southern Philippines since the Last Glacial Maximum. Chin. Sci. Bull. 56. http://dx.doi.org/10.1007/s11434-011-4573-1.

Bird, M.I., Taylor, D., Hunt, C., 2005. Palaeoenvironments of insular Southeast Asia during the Last Glacial Period: a savanna corridor in Sundaland? Quat. Sci. Rev. 24, 2228–2242.

Bobe, R., Behrensmeyer, A.K., 2004. The expansion of grassland ecosystems in Africa in relation to mammalian evolution and the origin of the genus Homo. Palaeogeogr. Palaeoclimatol. Palaeoecol. 207, 399–420.

Bray, E.E., Evans, E.D., 1961. Distribution of n-paraffins as a clue to recognition of source beds. Geochim. Cosmochim. Acta 22, 2–15. http://dx.doi.org/10.1016/0016-7037(61)90069-2.

Brincat, D., Yamada, K., Ishiwatari, R., Uemura, H., Naraoka, H., 2000. Molecular-isotopic stratigraphy of long-chain *n*-alkanes in Lake Baikal Holocene and glacial age sediments. Org. Geochem. 31, 287–294.

Buggle, B., Wiesenberg, G.L.B., Glaser, B., 2010. Is there a possibility to correct fossil n-alkane data for postsedimentary alteration effects? Appl. Geochem. 25, 947–957.

Calvo, E., Pelejero, C., Logan, G.A., De Deckker, P., 2004. Dust induced changes in phytoplankton composition in the Tasman Sea during the last four glacial cycles. Paleoceanography 19, PA2020. http://dx.doi.org/10.1029/2003PA000992.

Cane, M.A., Molnar, P., 2001. Closing of the Indonesian seaway as a precursor to east African aridification around 3 ± 4 million years ago. Nature 411, 157–162.

Carr, A.S., Boom, A., Chase, B.M., 2010. The potential of plant biomarker evidence derived from rock hyrax middens as an indicator of palaeoenvironmental change. Palaeogeogr. Palaeoclimatol. Palaeoecol. 285, 321–330.

Castañeda, I.S., Werne, J.P., Johnson, T.C., Filley, T.R., 2009. Late Quaternary vegetation history of southeast Africa: the molecular isotopic record from Lake Malawi. Palaeogeogr. Palaeoclimatol. Palaeoecol. 275, 100–112.

Chaisson, W.P., Ravelo, A.C., 2000. Pliocene development of the east-west hydrographic gradient in the equatorial Pacific. Paleoceanography 15, 497–505.

Chikaraishi, Y., Kaneko, M., Ohkouchi, N., 2012. Stable hydrogen and carbon isotopic compositions of long-chain (C_{21}–C_{33}) *n*-alkanes and *n*-alkenes in insects. Geochim. Cosmochim. Acta 95, 53–62.

Clemens, S.C., Prell, W.L., Sun, Y.B., Liu, Z.Y., Chen, G.S., 2008. Southern Hemisphere forcing of Pliocene $\delta^{18}O$ and the evolution of Indo–Asian monsoons. Paleoceanography 23, PA4201. http://dx.doi.org/10.1029/2008PA001638.

Clift, P.D., Hodges, K.V., Heslop, D., Hannigan, R., Van Long, H., Calves, G., 2008. Correlation of Himalayan exhumation rates and Asian monsoon intensity. Nat. Geosci. 1, 875–880.

Conte, M.H., Weber, J.C., 2002. Long-range atmospheric transport of terrestrial biomarkers to the western North Atlantic. Glob. Biogeochem. Cycles 16, 1142. http://dx.doi.org/10.1029/2002GB001922.

Cranwell, P.A., 1973. Chain-length distribution of *n*-alkanes from lake sediments in relation to post-glacial environmental change. Freshw. Biol. 3, 259–265.

Cranwell, P.A., Eglinton, G., Robinson, N., 1987. Lipids of aquatic organisms as potential contributors to lacustrine sediments. Org. Geochem. 11, 513–527.

Cui, J.W., Huang, J.H., Xie, S.C., 2008. Characteristics of seasonal variations of leaf n-alkanes and n-alkenes in modern higher plants in Qingjiang, Hubei Province, China. Chin. Sci. Bull. 53, 2659–2664. http://dx.doi.org/10.1007/s11434-008-0194-8.

De Deckker, P., Tapper, N.J., Van der Kaars, S., 2002. The status of the Indo-Pacific Warm Pool and adjacent land at the Last Glacial Maximum. Glob. Planet. Change 35, 25–35.

deMenocal, P.B., 2004. African climate change and faunal evolution during the Pliocene-Pleistocene. Earth Planet. Sci. Lett. 220, 3–24.

deMenocal, P.B., 2011. Climate and human evolution. Science 311, 540–541.

Diefendorf, A.F., Freeman, K.H., Wing, S.L., Graham, H.V., 2011. Production of *n*-alkyl lipids in living plants and implications for the geologic past. Geochim. Cosmochim. Acta 75, 7472–7485.

Ding, Z.L., Yang, S.L., Sun, J.M., Liu, T.S., 2001. Iron geochemistry of loess and red clay deposits in the Chinese Loess Plateau and implications for long-term Asian monsoon evolution in the last 7.0 Ma. Earth Planet. Sci. Lett. 185, 99–109.

Dodd, R.S., Afzal-Rafii, Z., 2000. Habitat-related adaptive properties of plant cuticular lipids. Evolution 54, 1438–1444.

Dodd, R.S., Poveda, M., 2003. Environmental gradients and population divergence contribute to variation in cuticular wax composition in *Juniperus communis*. Biochem. Syst. Ecol. 31, 1257–1270.

Duan, Y., He, J.X., 2011. Distribution and isotopic composition of n-alkanes from grass, reed and tree leaves along a latitudinal gradient in China. Geochem. J. 45, 199–207.

Eglinton, G., Hamilton, R.J., 1967. Leaf epicuticular waxes. Science 156, 1322–1335.

Eglinton, T.I., Eglinton, G., 2008. Molecular proxies for paleoclimatology. Earth Planet. Sci. Lett. 275, 1–16.

Feakins, S.J., deMenocal, P.B., Eglinton, T.I., 2005. Biomarker records of late Neogene changes in northeast African vegetation. Geology 33, 977–980.

Fedorov, A.V., Dekens, P.S., McCarthy, M., Ravelo, A.C., deMenocal, P.B., Barreiro, M., Pacanowski, R.C., Philander, S.G., 2006. The Pliocene paradox (mechanisms for a permanent El Niño). Science 312, 1485–1489.

Gagosian, R.B., Peltzer, E.T., 1986. The importance of atmospheric input of terrestrial organic material to deep sea sediments. Org. Geochem. 10, 661–669.

Gasse, F., 2000. Hydrological changes in the African tropics since the Last Glacial Maximum. Quat. Sci. Rev. 19, 189–211.

Gogou, A., Bouloubassi, I., Stephanou, E.G., 2000. Marine organic geochemistry of the Eastern Mediterranean: 1. Aliphatic and polyaromatic hydrocarbons in Cretan Sea surficial sediments. Mar. Chem. 68, 265–282.

Hanebuth, T.J.J., Stattegger, K., 2004. Depositional sequences on a late Pleistocene–Holocene tropical siliciclastic shelf (Sunda Shelf, Southeast Asia). J. Asian Earth Sci. 3, 113–126.

Hanisch, S., Ariztegui, D., Püttmann, W., 2003. The biomarker record of Lake Albano, central Italy – implications for Holocene aquatic system response to environmental change. Org. Geochem. 34, 1223–1235.

Haug, G.H., Tiedemann, R., 1998. Effect of the formation of the Isthmus of Panama on Atlantic Ocean thermohaline circulation. Nature 393, 673–676.

He, J., Zhao, M.X., Li, L., Wang, P.X., Ge, H.M., 2008. Sea surface temperature and terrestrial biomarker records of the last 260 ka of core MD05-2904 from the northern South China Sea. Chin. Sci. Bull. 53, 2376–2384.
Heaney, L.R., 1991. A synopsis of climatic and vegetational changes in Southeast Asia. Clim. Change 19, 53–61.
Hedges, J.I., Prahl, F.G., 1993. Early diagenesis: consequences for applications of molecular biomarkers. In: Engel, M.H., Macko, S.A. (Eds.), Organic Geochemistry: Principles and Applications. Plenum Press, New York, pp. 237–253.
Hiscott, R.N., 2001. Depositional sequences controlled by high rates of sediment supply, sea-level variations, and growth faulting: the Quaternary Baram Delta of northwestern Borneo. Mar. Geol. 175, 67–102.
Hönisch, B., Hemming, N.G., Archer, D., Siddall, M., McManus, J.F., 2009. Atmospheric carbon dioxide concentration across the mid-Pleistocene transition. Science 324, 1551–1554.
Horikawa, K., Murayama, M., Minagawa, M., Kato, Y., Sagawa, T., 2010. Latitudinal and downcore (0–750 ka) changes in *n*-alkane chain lengths in the eastern equatorial Pacific. Quat. Res. 73, 573–582.
Hu, D., Böning, P., Köhler, C.M., Hillier, S., Pressling, N., Wan, S., Brumsack, H.-J., Clift, P.D., 2012. Deep sea records of the continental weathering and erosion response to East Asian monsoon intensification since 14ka in the South China Sea. Chem. Geol. 326–327, 1–18. http://dx.doi.org/10.1016/j.chemgeo.2012.07.024.
Hu, J.F., Peng, P.A., Fang, D.Y., Jia, G.D., Jian, Zh.M., Wang, P.X., 2003. No aridity in Sunda Land during the Last Glaciation: evidence from molecular-isotopic stratigraphy of long-chain *n*-alkanes. Palaeogeogr. Palaeoclimatol. Palaeoecol. 201, 269–281.
Huang, X.Y., Xue, J.T., Zhang, J.X., Qin, Y.M., Meyers, P.A., Wang, H.M., 2012. Effect of different wetness conditions on Sphagnum lipid composition in the Erxianyan peatland, central China. Org. Geochem. 44, 1–7.
Huang, Y.S., Clemens, S.C., Liu, W.G., Wang, Y., Prell, W.L., 2007. Large-scale hydrological change drove the late Miocene C_4 plant expansion in the Himalayan foreland and Arabian Peninsula. Geology 35, 531–534.
Hughen, K.A., Eglinton, T.I., Xu, L., Makou, M., 2004. Abrupt tropical vegetation response to rapid climate changes. Science 304, 1955–1959.
Jansen, B., Haussmann, N.S., Tonneijck, F.H., Verstraten, J.M., de Voogt, P., 2008. Characteristic straight-chain lipid ratios as a quick method to assess past forest–páramo transitions in the Ecuadorian Andes. Palaeogeogr. Palaeoclimatol. Palaeoecol. 262, 129–139.
Jeng, W.-L., 2006. Higher plant *n*-alkane average chain length as an indicator of petrogenic hydrocarbon contamination in marine sediments. Mar. Chem. 102, 242–251.
Jiang, H.C., Ding, Z.L., 2008. A 20 Ma pollen record of East-Asian summer monsoon evolution from Guyuan, Ningxia, China. Palaeogeogr. Palaeoclimatol. Palaeoecol. 265, 30–38.
Kawamura, K., Ishimura, Y., Yamazaki, K., 2003. Four years' observations of terrestrial lipid class compounds in marine aerosols from the western North Pacific. Glob. Biogeochem. Cycles 17, 1003. http://dx.doi.org/10.1029/2001GB001810.
Lane, C.S., Horn, S.P., Mora, C.I., Ovis, K.H., Finkelstein, D.B., 2011. Sedimentary stable carbon isotope evidence of late Quaternary vegetation and climate change in highland Costa Rica. J. Paleolimnol. 45, 323–338.
Laskar, J., Robutel, P., Joutel, F., Gastineau, M., Correia, A.C.M., Levrard, B., 2004. A long term numerical solution for the insolation quantities of the Earth. Astron Astrophys. 428, 261–285. http://dx.doi.org/10.1051/0004-6361:20041335.
Lawrence, K.T., Liu, Z.H., Herbert, T.D., 2006. Evolution of the eastern tropical Pacific through Plio-Pleistocene glaciation. Science 312, 79–83.
Levin, N.E., Quade, J., Simpson, S.W., Semaw, S., Rogers, M., 2004. Isotopic evidence for Plio-Pleistocene environmental change at Gona, Ethiopia. Earth Planet. Sci. Lett. 219, 93–110.
Li, F.J., Wu, N.Q., 2010. Pliocene land snail record from western Chinese Loess Plateau and implications for impacts of the summer insolation gradient between middle and low latitudes on the East Asian summer monsoon. Glob. Planet. Change 72, 73–78.
Li, L., Li, Q.Y., Tian, J., Wang, P.X., Wang, H., Liu, Z.H., 2011. A 4-Ma record of thermal evolution in the tropical western Pacific and its implications on climate change. Earth Planet. Sci. Lett. 309, 10–20.
Liu, T.S., Ding, Z.L., 1993. Stepwise coupling of monsoon circulation to global ice volume variations during the late Cenozoic. Glob. Planet. Change 7, 119–130.
Liu, W.G., Huang, Y.S., 2005. Compound-specific D/H ratios and molecular distributions of higher plant leaf waxes as novel paleoenvironmental indicators in the Chinese Loess Plateau. Org. Geochem. 36, 851–860.
Liu, Z.F., Colin, C., Trentesaux, A., Blamart, D., Bassinot, F., Siani, G., Sicre, M., 2004. Erosional history of the eastern Tibetan Plateau since 190 kyr ago: clay mineralogical and geochemical investigations from the southwestern South China Sea. Mar. Geol. 209, 1–18.
Liu, Z.Y., 2011. Glacial cycles and Indian Monsoon – a southern push. Science 333, 706–708.
Lunt, D.J., Foster, G.L., Haywood, A., Stone, E.J., 2008. Late Pliocene Greenland glaciation controlled by a decline in atmospheric CO_2 levels. Nature 454, 1102–1105.
Marlow, J.R., Lange, C.B., Wefer, G., Rosell-Mele, A., 2000. Upwelling intensification as part of the Pliocene–Pleistocene climate transition. Science 290, 2288–2291.
Martínez-Garcia, A., Rosell-Melé, A., Jaccard, S.L., Geibert, W., Sigman, D.M., Haug, G.H., 2011. Southern Ocean dust-climate coupling over the past four million years. Nature 476, 312–316.
Mazurek, M.A., Cass, G.R., Simoneit, B.R.T., 1989. Interpretation of high-resolution gas chromatography and high-resolution gas chromatography/mass spectrometry data acquired from atmospheric organic aerosol samples. Aerosol Sci. Technol. 10, 408–420.
McLaren, S., Wallace, M.W., 2010. Plio-Pleistocene climate change and the onset of aridity in southeastern Australia. Glob. Planet. Change 71, 55–72.
Medina, E., Aguiar, G., Gómez, M., Aranda, J., Medina, J.D., Winter, K., 2006. Taxonomic significance of the epicuticular wax composition in species of the genus *Clusia* from Panama. Biochem. Syst. Ecol. 34, 319–326.
Meyers, P.A., Ishiwatari, R., 1993. Lacustrine organic geochemistry: an overview of indicators of organic matter sources and diagenesis in lake sediments. Org. Geochem. 20, 867–900.
Milliman, J.D., Meade, R.H., 1983. World wide delivery of river sediment to the oceans. J. Geol. 91, 1–21.
Molengraaff, G.A.F., Weber, M., 1920. On the relation between the Pleistocene glacial period and the origin of the Sunda Sea (Java- and South China-Sea), and its influence on the distribution of coral reefs and on the land- and freshwater fauna. Proc. R. Acad. 23, 394–428.
Molnar, P., Boos, W.R., Battisti, D.S., 2010. Orographic controls on climate and paleoclimate of Asia: thermal and mechanical roles for the Tibetan Plateau. Annu. Rev. Earth Planet. Sci. 38, 77–102.
Ohkouchi, N., Kawamura, K., Kawahata, H., Taira, A., 1997. Latitudinal distributions of terrestrial biomarkers in the sediments from the Central Pacific. Geochim. Cosmochim. Acta 61, 1911–1918.
Pagani, M., Liu, Z.H., LaRiviere, J., Ravelo, A.C., 2010. High Earth-system climate sensitivity determined from Pliocene carbon dioxide concentrations. Nat. Geosci. 3, 27–30.
Paillard, D., Labeyrie, L., Yiou, P., 1996. Macintosh program performs time-series analysis. Eos Trans. Am. Geophys. Union 77, 379.
Pelejero, C., 2003. Terrigenous *n*-alkane input in the South China Sea: high-resolution records and surface sediments. Chem. Geol. 200, 89–103.
Pelejero, C., Kienast, M., Wang, L., Grimalt, J.O., 1999. The flooding of Sundaland during the last deglaciation: imprints in hemipelagic sediments from the southern South China Sea. Earth Planet. Sci. Lett. 171, 661–671.
Poynter, J.G., Eglinton, G., 1990. Molecular composition of three sediments from Hole 717C: the Bengal Fan. Proc. Ocean Drill. Prog. Sci. Results 116, 155–161.
Poynter, J.G., Farrimond, P., Robinson, N., Eglinton, G., 1989. Aeolian-derived higher plant lipids in the marine sedimentary record: links with palaeoclimate. In: Leine, M., Sarnthein, M. (Eds.), Modern and Past Patterns of Global Atmospheric Transport. Kluwer Academic Publishers, Norwell, pp. 435–462.
Rao, Z.G., Wu, Y., Zhu, Z.Y., Jia, G.D., Henderson, A., 2011. Is the maximum carbon number of long-chain *n*-alkanes an indicator of grassland or forest? Evidence from surface soils and modern plants. Chin. Sci. Bull. 56. http://dx.doi.org/10.1007/s11434-011-4418.
Ratnayake, N.P., Suzuki, N., Okada, M., Takagi, M., 2006. The variations of stable carbon isotope ratio of land plant-derived *n*-alkanes in deep-sea sediments from the Bering Sea and the North Pacific Ocean during the last 250,000 years. Chem. Geol. 228, 197–208.
Ravelo, A.C., Andreasen, D.H., Lyle, M., Lyle, A.O., Wara, M.W., 2004. Regional climate shifts caused by gradual global cooling in the Pliocene epoch. Nature 429, 263–267.
Raymo, M.E., Nisancioglu, K., 2003. The 41 kyr world: Milankovitch's other unsolved mystery. Paleoceanography 18. http://dx.doi.org/10.1029/2002PA000791.
Raymo, M.E., Grant, B., Horowitz, M., Rau, G.H., 1996. Mid-Pliocene warmth: stronger greenhouse and stronger conveyer. Mar. Micropaleo. 27, 313–326.
Raymo, M.E., Lisiecki, L.E., Nisancioglu, K.H., 2006. Plio-Pleistocene ice volume, Antarctic climate, and the global $\delta^{18}O$ record. Science 28, 492–495.
Rea, D.K., 1992. Delivery of Himalayan sediment to the northern Indian Ocean and its relation to global climate, sea level, uplift, and seawater strontium. In: Duncan, R.A., Rea, D.K., Kidd, R.B., von Rad, U., Weissel, J.K. (Eds.), Synthesis of Results from Scientific Drilling in the Indian Ocean, American Geophysical Union Geophysical Monograph, vol. 70, pp. 387–402.
Rea, D.K., Snoeckx, H., Joseph, L.H., 1998. Late Cenozoic eolian deposition in the North Pacific: Asian drying, Tibetan uplift, and cooling of the northern hemisphere. Paleoceanography 13, 215–224.
Rommerskirchen, F., Eglinton, G., Dupont, L., Güntner, U., Wenzel, C., Rullkötter, J., 2003. A north to south transect of Holocene southeast Atlantic continental margin sediments: relationship between aerosol transport and compound-specific $\delta^{13}C$ land plant biomarker and pollen records. Geochem. Geophys. Geosyst. 4, 1101. http://dx.doi.org/10.1029/2003GC000541.
Rommerskirchen, F., Eglinton, G., Dupont, L., Rullkötter, J., 2006a. Glacial/interglacial changes in southern Africa: compound-specific $\delta^{13}C$ land plant biomarker and pollen records from southeast Atlantic continental margin sediments. Geochem. Geophys. Geosyst. 7, Q08010. http://dx.doi.org/10.1029/2005GC001223.
Rommerskirchen, F., Plader, A., Eglinton, G., Chikaraishi, Y., Rullkötter, J., 2006b. Chemotaxonomic significance of distribution and stable carbon isotopic composition of long-chain alkanes and alkan-1-ols in C-4 grass waxes. Org. Geochem. 37, 1303–1332.
Sachse, D., Radke, J., Gleixner, G., 2006. δD values of individual *n*-alkanes from terrestrial plants along a climatic gradient-implications for the sedimentary biomarker record. Org. Geochem. 37, 469–483.
Schefuß, E., Ratmeyer, V., Stuut, J.-B.W., Jansen, J.H.F., Sinninghe Damsté, J.S., 2003. Carbon isotope analyses of *n*-alkanes in dust from the lower atmosphere over the central eastern Atlantic. Geochim. Cosmochim. Acta 67, 1757–1767.
Schwark, L., Zink, K., Lechterbeck, J., 2002. Reconstruction of postglacial to early Holocene vegetation history in terrestrial Central Europe via cuticular lipid biomarkers and pollen records from lake sediments. Geology 30, 463–466.

Seki, O., Nakatsuka, T., Shibata, H., Kawamura, K., 2010. A compound-specific *n*-alkane $\delta^{13}C$ and δD approach for assessing source and delivery processes of terrestrial organic matter within a forested watershed in northern Japan. Geochim. Cosmochim. Acta 74, 599–613.

Seki, O., Yoshikawa, C., Nakatsuka, T., Kawamura, K., Wakatsuchi, M., 2006. Fluxes, source and transport of organic matter in the western Sea of Okhotsk: stable carbon isotopic ratios of *n*-alkanes and total organic carbon. Deep-Sea Res. I 53, 253–270.

Sendjaja, Y.A., Kimura, J.I., 2010. Geochemical variation in Tertiary–Quaternary lavas of the West Java arc, Indonesia steady-state subduction over the past 10 million years. J. Mineral. Petrol. Sci. 105, 20–28.

Shintani, T., Yamamoto, M., Chen, M.T., 2011. Paleoenvironmental changes in the northern South China Sea over the past 28,000 years: A study of TEX86-derived sea surface temperatures and terrestrial biomarkers. J. Asian Earth Sci. 40, 1221–1229.

Simoneit, B.R.T., Sheng, G.Y., Chen, X.J., Fu, J.M., Zhang, J., Xu, Y., 1991. Molecular marker study of extractable organic matter in aerosols from urban areas of China. Atmos. Environ. 25A, 2111–2129.

Sun, X.J., Li, X., Luo, Y.L., Chen, X.D., 2000. The vegetation and climate at the last glaciation on the emerged continental shelf of the South China Sea. Palaeogeogr. Palaeoclimatol. Palaeoecol. 160, 301–316.

Sun, X.J., Luo, Y.L., Huang, F., Tian, J., Wang, P.X., 2003. Deep-sea pollen from the South China Sea: Pleistocene indicators of East Asian monsoon. Mar. Geol. 201, 97–118.

Sun, Y.B., An, Z.S., Clemens, S.C., Bloemendal, J., Vandenberghe, J., 2010. Seven million years of wind and precipitation variability on the Chinese Loess Plateau. Earth Planet. Sci. Lett. 297, 525–535.

Sun, Y.B., Clemens, S.C., An, Z.S., Yu, Z.W., 2006. Astronomical timescale and palaeoclimatic implication of stacked 3.6-Myr monsoon records from the Chinese Loess Plateau. Quat. Sci. Rev. 25, 33–48.

Tian, J., Wang, P.X., Chen, X.R., Li, Q.Y., 2002. Astronomically tuned Plio-Pleistocene benthic $\delta^{18}O$ records from South China Sea and Atlantic-Pacific comparison. Earth Planet. Sci. Lett. 203, 1015–1029.

Tian, J., Wang, P.X., Chen, X.R., 2004. Development of the East Asian monsoon and Northern Hemisphere glaciation: oxygen isotope records from the South China Sea. Quat. Sci. Rev. 23, 2007–2016.

Trauth, M.H., Maslin, M.A., Deino, A., Strecker, M.R., 2005. Late Cenozoic moisture history of East Africa. Science 309, 2051–2053.

Trauth, M.H., Maslin, M.A., Deino, A., Strecker, M.R., Bergner, A.G.N., Dühnforth, M., 2007. High- and low-latitude forcing of Plio-Pleistocene African climate and human evolution. J. Hum. Evol. 53, 475–486.

Vogts, A., Schefuß, E., Badewien, T., Rullkötter, J., 2012. *n*-Alkane parameters from a deep sea sediment transect off southwest Africa reflect continental vegetation and climate conditions. Org. Geochem. 47, 109–119.

Wan, S.M., Li, A.C., Clift, P.D., Jiang, H.Y., 2006. Development of the East Asian summer monsoon: evidence from the sediment record in the South China Sea since 8.5 Ma. Palaeogeogr. Palaeoclimatol. Palaeoecol. 241, 139–159.

Wan, S.M., Tian, J., Steinke, S., Li, A.C., Li, T.G., 2010. Evolution and variability of the East Asian summer monsoon during the Pliocene: evidence from clay mineral records of the South China Sea. Palaeogeogr. Palaeoclimatol. Palaeoecol. 293, 237–247.

Wang, P.X., 1999. Response of Western Pacific marginal seas to glacial cycles: paleoceanographic and sedimentological features. Mar. Geol. 156, 5–39.

Wang, P.X., Li, Q.Y., 2009. The South China Sea: Paleoceanography and Sedimentology. Springer.

Wang, P.X., Prell, W.L., Blum, P., 2000. Initial Reports 184, Ocean Drilling Program. In: Proceedings of the Ocean Drilling Program. Texas Agricultural and Mechanical University, College Station TX 77845–79547, USA.

Wang, P.X., Tian, J., Lourens, L.J., 2010. Obscuring of long eccentricity cyclicity in Pleistocene oceanic carbon isotope records. Earth Planet. Sci. Lett. 290, 319–330.

Wang, X.M., Sun, X.J., Wang, P.X., Stattegger, K., 2009. Vegetation on the Sunda Shelf, South China Sea, during the Last Glacial Maximum. Palaeogeogr. Palaeoclimatol. Palaeoecol. 278, 88–97.

Wang, Y.L., Fang, X.M., Zhang, T.W., Li, Y.M., Wu, Y.Q., He, D.X., Gao, Y., Meng, P., Wang, Y.X., 2012. Distribution of biomarkers in lacustrine sediments of the Linxia Basin, NE Tibetan Plateau, NW China: significance for climate change. Sediment. Geol. 243–244, 108–116.

Wara, M.W., Ravelo, A.C., Delaney, M.L., 2005. Permanent El Niño-like conditions during the Pliocene warm period. Science 309, 758–761.

Wehausen, R., Tian, J., Brumsack, H.J., Cheng, X.R., Wang, P.X., 2003. Geochemistry of Pliocence sediments from ODP site 1143 (Southern South China Sea). In: Wang, P., Prell, W.L., et al. (Eds.), Proceedings of the Ocean Drilling Program, Science Results, vol. 184, pp. 1–25. Available from: http://www-odp.tamu.edu/publications/184_SR/VOLUME/CHAPTERS/201.PDF.

Wu, N.Q., Pei, Y.P., Lu, H.Y., Guo, Z.T., Li, F.J., Liu, T.S., 2006. Marked ecological shifts during 6.2–2.4 Ma revealed by a terrestrial molluscan record from the Chinese Red Clay Formation and implication for palaeoclimatic evolution. Palaeogeogr. Palaeoclimatol. Palaeoecol. 233, 287–299.

Xie, S.C., Yi, Y., Liu, Y.Y., Gu, Y.S., Ma, Z.X., Lin, W.J., Wang, X.Y., Liu, G., Liang, B., Zhu, Z.M., 2003. The Pleistocene vermicular red earth in South China signaling the global climatic change: the molecular fossil record. Sci. China (Ser. D) 46, 1113–1120.

Xiong, S.F., Ding, Z.L., Zhu, Y.J., Zhou, R., Lu, H.J., 2010. A-6Ma chemical weathering history, the grain size dependence of chemical weathering intensity, and its implications for provenance change of the Chinese loess –red clay deposit. Quat. Sci. Rev. 29, 1911–1922.

Yamamoto, S., Kawamura, K., Seki, O., Meyers, P.A., Zheng, Y.H., Zhou, W.J., 2010. Environmental influences over the last 16 ka on compound-specific $\delta^{13}C$ variations of leaf wax *n*-alkanes in the Hani peat deposit from northeast China. Chem. Geol. 277, 261–268.

Zachos, J., Pagani, M., Sloan, L., Thomas, E., Billups, K., 2001. Trends, rhythms, and aberrations in global climate 65 Ma to Present. Science 292, 686–693.

Zech, M., 2006. Evidence for Late Pleistocene climate changes from buried soils on the southern slopes of Mt. Kilimanjaro, Tanzania. Palaeogeogr. Palaeoclimatol. Palaeoecol. 242, 303–312.

Zech, M., Zech, R., Morrás, H., Moretti, L., Glaser, B., Zech, W., 2009. Late Quaternary environmental changes in Misiones, subtropical NE Argentina, deduced from multi-proxy geochemical analyses in a palaeosol-sediment sequence. Quat. Int. 196, 121–136.

Zhang, Y.G., Ji, J.F., Balsam, W., Liu, L.W., Chen, J., 2009. Mid-Pliocene Asian monsoon intensification and the onset of Northern Hemisphere glaciation. Geology 37, 599–602.

Zhang, Z.H., Zhao, M.X., Eglinton, G., Lu, H., Huang, C.Y., 2006. Leaf wax lipids as paleovegetational and paleoenvironmental proxies for the Chinese Loess Plateau over the last 170 kyr. Quat. Sci. Rev. 25, 575–594.

Zheng, H.B., Powell, C.A., An, Z.S., Zhou, J., Dong, G., 2000. Pliocene uplift of the northern Tibetan Plateau. Geology 28, 715–718.

Zheng, H.B., Powell, C.M., Rea, D.K., Wang, J.L., Wang, P.X., 2004. Late Miocene and mid-Pliocene enhancement of the East Asian monsoon as viewed from the land and sea. Glob. Planet. Change 41, 147–155.

Zheng, Y.H., Zhou, W.J., Meyers, P.A., Xie, S.C., 2007. Lipid biomarkers in the Zoigę-Hongyuan peat deposit: indicators of Holocene climate changes in West China. Org. Geochem. 38 (11), 1927–1940.

Zheng, Y.H., Zhou, W.J., Xie, S.C., Yu, X.F., 2009. A comparative study of *n*-alkane biomarker and pollen records: an example from southern China. Chin. Sci. Bull. 54, 1065–1072. http://dx.doi.org/10.1007/s11434-008-0563-3.

Zhou, B., Zheng, H.B., Yang, W.G., Taylor, D., Lu, Y.H., Wei, G.J., Li, L., Wang, H., 2012. Climate and vegetation variations since the LGM recorded by biomarkers from a sediment core in the northern South China Sea. J. Quat. Sci. 27, 948–955.

Zhou, W.J., Xie, S.C., Meyers, P.A., Zheng, Y.H., 2005. Reconstruction of late glacial and Holocene climate evolution in southern China from geolipids and pollen in the Dingnan peat sequence. Org. Geochem. 36, 1272–1284.